REVIEW

Check for updates

Recent applications of coinage metal nanoparticles passivated with salicylaldehyde and salicylaldehyde-based Schiff bases

Mamta Sahu, Mainak Ganguly [ID] * and Priyanka Sharma

Salicylaldehyde (SD) and its derivatives are effective precursors for generating coinage metal (gold, silver, and copper) nanoparticles (NPs). These NPs have a variety of potential environmental applications, such as in water purification and sensing, and those arising from their antibacterial activity. The use of SD and its derivatives for synthesizing coinage NPs is attractive due to several factors. First, SD is a relatively inexpensive and readily available starting material. Second, the synthetic procedures are typically simple and can be carried out under mild conditions. Finally, the resulting NPs can be tailored to have specific properties, such as size, shape, and surface functionality, by varying the reaction conditions. In an alkaline solution, the phenolate form of SD was converted to its quinone form, while ionic coinage metal salts were converted to zero-valent nanoparticles. The capping *in situ* produced quinone of coinage metal nanoparticles generated metal-enhanced fluorescence under suitable experimental conditions. The formation of iminic bonds during the formation of Schiff bases altered the properties (especially metal-enhanced fluorescence) and applications.

1. Motivation

The study highlights the advantages of using SD for synthesizing and capping coinage metal nanoparticles (CNPs). Cost-effectiveness, small size, ease of use, and capability of manipulating the plasmonic behavior made SD an interesting research material. SD is commonly used to form chelating metal complexes.[1] Maher and Mohammed reviewed SD and SD derivatives for metal complex formation. However, no review article is available on SD-capped NPs with versatile applications including metal-enhanced fluorescence (due to manipulation of plasmonic mode density). CNPs with SD capping have been well studied. The condensation reaction with various amines produced Schiff bases with iminic bonds contributing a new milestone in the application of CNPs. Under these circumstances, we concentrated on writing a critical review article on SD and SD-based Schiff bases in nanoscience.

Department of Chemistry, Solar Energy Conversion and Nanomaterials Laboratory, Manipal University Jaipur, Dehmi Kalan, Jaipur 303007, Rajasthan, India. E-mail: humansense2009@gmail.com

Mamta Sahu received her BSc degree from S. S. Jain Subodh Girls PG College (Jaipur, India) and MSc from R. K. Vigyan Mahavidyalya (Jaipur, India). She is currently pursuing her PhD degree under the supervision of Dr Mainak Ganguly in the Department of Chemistry at Manipal University Jaipur (India). Her area of research is environmental nanoscience and spectroscopy.

Mamta Sahu

Dr Mainak Ganguly received his PhD from the Indian Institute of Technology, Kharagpur India in 2014. He also had 5 years of postdoctoral research experience at Furman University (USA) and McGill University (Canada). He is currently working as an assistant professor in the Department of Chemistry, Manipal University Jaipur (India). His research interests include nanoparticles, clusters, biophysical chemistry, environmental remediation, etc. He has published more than 60 papers.

Mainak Ganguly

2. Introduction

Biotechnology, materials science, computer science, health, pharmacy, and engineering are all involved in nanotechnology, which focuses on materials at 10^{-9} meter scales. Due to their widespread applications in commercial settings, NPs in both crystalline and amorphous forms have drawn much attention worldwide. This has encouraged several research institutes to focus on creating and growing a range of nano-applications.[2,3] A capping agent can function as both a "poison" restricting access to active sites and a "promoter" increasing yields and controlling selectivity unexpectedly. These effects can be attributed to the formation of an interphase between metals and ligands, which have special characteristics that drive catalysis. Thus, it is crucial to comprehend this interphase structure to optimize the design of customized nanocatalysts.[4,5] SD, also known as 2-hydroxybenzaldehyde, is a simple, naturally occurring reagent that is inexpensive and easily available. The price per kilogram at Sigma-Aldrich is $341. SD fluoresces very faintly because of its comparatively small π-conjugated benzene ring structure.[6] SD is a capping agent that contributes both directly and indirectly to the production of nanoparticles.[7,8] SD is used as a sensing probe and for elimination of toxic materials, with CNPs. Nowadays, SD is also used for metal enhanced fluorescence (MEF), placing CNPs in perfect proximity.[8]

With little change in the capping agent, we can get drastic changes in the physicochemical properties of NPs. SD can be converted into a Schiff base *via* the condensation reaction of amines with the formation of iminic bonds. Schiff base (obtained from SD) capped NPs are used for many applications, for example sensing and antibacterial activity.

CNPs, which include gold, silver, and copper, exhibit special optical characteristics due to localized surface plasmon resonance (LSPR), which makes them a great option for sensor applications.[9] In addition to causing higher local electromagnetic fields close to the nanoparticle's surface, LSPR is the cause of the strong absorption band that the particle exhibits. Because LSPR is dependent on both the nanoparticle and the medium in which it is disseminated, it may be adjusted by adjusting the composition, size, form, and dielectric characteristics of the surrounding medium of the nanoparticles.[10] The interparticle distance between pairs of NPs affects the surface plasmon characteristics of metal nanoparticles as well. As NPs approach one another under the influence of an analyte, their electric fields interact, causing interparticle plasmon coupling, which in turn causes a coupling-induced LSPR shift and perceptible color changes.[10]

This review emphasizes the synthesis process of SD and SD-based Schiff-capped CNPs, their applications, and the fate of the involved elements. This suggests that the current study might be filling a gap in existing knowledge.

3. Coinage metal nanoparticles

Three nonradioactive elements from group 11 of the periodic table—Cu, Ag, and Au—have historically been used to manufacture the majority of coinage metals (or alloys). Cu is often augmented with Sn and other metals to create bronze. The ancient world's money was made of gold, silver, bronze, or copper, as was the majority of medieval coinage. Around 650 BC, Aegina Island, Ephesus, and Lydia were the starting points of all Western currency histories. In approximately the sixth century BC, ancient India became among the first issuers. Coins have been the most widely used representation of money ever since. To create the first currency, electrum, a naturally occurring creamy mixture of Ag and Au, was doped with a different metal.[11,12]

The term "coinage", however, is not entirely defined because other metals have already been used to make "demonstration coins", which have never been used to make any monetized nation-state currencies. They could come in handy later on. Although some of these elements (like zirconium) would make excellent coins in theory, it is unclear where these elements stand in terms of coin metals. Because coin metal is fundamentally costly, there is a significant challenge. The twenty-first century has seen several initiatives throughout the world advocating for the use of the least expensive and uncommon types of coinage metals. Tee and Ye provided an overview of the latest advancements in coinage metals within the nanoscale realm and their biological applications.[7,11]

From a historical standpoint, coinage metals are most renowned for their monetary, ornamental, and metallurgical merits; nevertheless, as nanotechnology's potential has only just come to light, their metal nanostructures and uses may be viewed as creations of modern science. Notable characteristics of coinage metal nanostructures include visual, electrical, chemical, and catalytic qualities that depend on form and size. Considerable research has been conducted on the creation and synthesis of coinage metal nanostructures and their possible uses because of each of these characteristics.[11] Numerous publications on using Cu, Ag, and Au catalysts to produce heterocycles can be found in the literature.[13] When formed as nanostructures, the metals Ag, Au, and Cu are known to display localized surface plasmon resonance (LSPR) peaks in the visible range.[14] Antibacterial metals like Cu, Ag, and Au may generally be employed as a kind of antibacterial agent.[15–17]

4. Salicylaldehyde

SD is a widely used, highly functionalized analyte, frequently used as a precursor to other chemicals. In analytical chemistry,

Priyanka Sharma received her BSc and MSc degrees from Maharaja Brij University, India. She is currently pursuing her PhD degree under the supervision of Dr Mainak Ganguly in the Department of Chemistry, at Manipal University Jaipur (India). Her areas of interest are materials science and environmental remediation.

Priyanka Sharma

SD is used for many different applications. For example, it may detect hydrazine and be used to make saligenin, coumarin, and salicylaldoxime, important analytical reagents. Moreover, SD contributes to taste and is an essential building block for several chelating agents.[7] Preservatives like SD and its derivatives are frequently found in perfumes, cosmetics, and essential oils.[7] SD is a widely used important chemical in many industrial processes, particularly in the large-scale manufacturing of medicines.

It has two distinct active functional groups, an aldehyde group and a hydroxy group. Due to their commercial availability and ease of access, SD and most of its derivatives are perfect starting materials for multicomponent reactions, primarily in pseudo-three and four-component ones that result in a wide variety of heterocyclic systems.[7] Before the introduction of a torsional twist of the substituent groups, the SD molecule was thought to have C_s symmetry.[18]

SD is frequently employed to produce chelating metal complexes.[1] Maher and Mohammed studied SD and its derivatives for metal complex formation. When SD condenses with amines, it produces chelating ligands. It condenses with ethylenediamine to provide the ligand 'salen'. Salicylaldoxime is produced with hydroxylamine. Catechol (1,2-dihydroxybenzene) is produced by oxidation with hydrogen peroxide (Dakin reaction) {Dakin, 1923 #47}. An aldol condensation produces the derivative of the heterocycle coumarin upon condensation with diethyl malonate.[1]

4.1 Fluorescence properties of salicylaldehyde

Properties of protonated SD have been studied both theoretically and experimentally using *ab initio* calculations. This aromatic molecule has two functional groups: a hydroxyl group (OH as in phenol) and an aldehyde group (CHO as in benzaldehyde). With intramolecular hydrogen bonding between the hydroxyl and carbonyl groups, neutral SD is a model molecule that displays an excited-state intramolecular proton transfer (ESIPT) reaction. Experimental methods and theoretical methods have been used extensively to study the intramolecular proton transfer process in the lowest singlet[19] states (S0, S1, and S2).[20,21] The rotation of the aldehyde group around the C–C bond and the hydroxyl group's *cis–trans* location about the aldehyde group result in a variety of conformers for protonated SD.[20] Many functionalized SD derivatives have been synthesized under a range of conditions. Their photophysical properties and solid-state/solution phase fluorescence intensities are quite promising.[22]

Synthetic intermediates known as SD derivatives have been extensively documented in the literature as the first steps towards developing Schiff bases,[7] salen-based probes,[19] and other heterocycles.[23] They benefit from being readily accessible commercial reagents at a low cost or being attainable through a restricted number of synthesis steps. Moreover, a recent case brought out the use of unsubstituted deprotonated SD as a photocatalyst relying on visible light.[6] However, unlike acetophenone or benzophenone analogs,[22] SD derivatives display
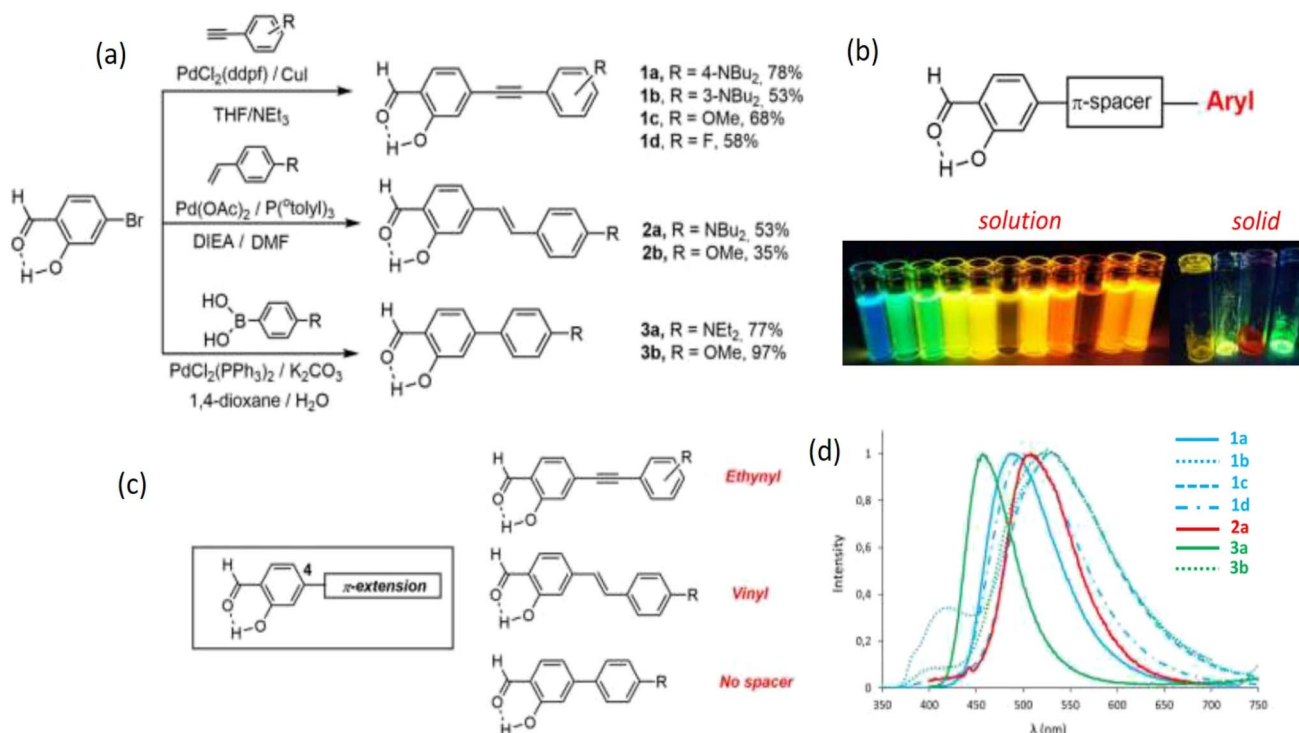

Fig. 1 (a) Synthesis protocol of 4-extended SD derivatives **1a–d**, **2a–b**, and **3a–b**. (b) Compounds of SD that exhibit intense fluorescence in multiple environments in solution and solid state. (c) 4-Extended SD derivatives. (d) SD's emission spectra in aerated solutions of toluene at room temperature are as follows: **1a** (plain blue), **1b** (dotted blue), **1c** (dashed blue), **1d** (dotted dashed blue), **2a** (plain red), **2b** (dotted red), **3a** (plain green), and **3b** (dotted green). Reproduced with permission from ref. 22, copyright 2024, *Eur. J. Org. Chem.*

Table 1 Compilation of the photophysical characteristics of SD derivatives **1a–d**, **2a–b**, and **3a–b** in solution. Reproduced with permission from ref. 22, copyright 2024, *Eur. J. Org. Chem.*

Dye	λ_{abs} (nm)	ε (M^{-1} cm^{-1})	λ_{em} (nm)	ΔS^b (cm^{-1})	$\Phi_F{}^a$	τ (ns)	$K_r{}^c$	$K_{nr}{}^c$	Solvent
1a	412	33 000	424	690	0.53	1.3	4.08	3.62	CH^d
1a	407	31 000	490	4200	0.68	3.1	2.19	1.03	Toluene
1a	398	42 300	508	5400	0.60	3.4	1.76	1.18	Et$_2$O
1a	401	33 000	555	6900	0.11	2.5	0.44	3.56	THF
1a	411	38 000	605	7800	0.02	0.6	0.33	16.30	CH$_2$Cl$_2$
1a	351	11 600	533	9700	0.01	0.4	0.25	24.80	CH$_2$Cl$_2$/H$^+$
1a	400	30 800	e	e	e	e	e	e	Acetone
1a	400	27 000	e	e	e	e	e	e	CH$_3$CN
1a	401	25 500	442/594	2300	0.01	0.5	0.20	19.80	DMSO
1a	400	30 400	587	8000	0.02	0.4	0.50	24.50	DMF
1b	393	25 100	445	3000	0.12	2.3	0.53	3.83	CH^d
1b	388	26 200	506	6000	0.29	10.0	0.29	0.71	Toluene
1b	389	25 400	410/605	9200	0.06	4.1	0.15	2.29	THF
1b	394	28 300	654	10 100	0.02	1.7	0.12	5.76	CH$_2$Cl$_2$
1b	348	34 100	533	10 000	0.01	0.8	0.13	12.40	CH$_2$Cl$_2$/H$^+$
1c	346	26 800	424/532	5300	0.01	0.5	0.20	19.80	Toluene
1d	320	30 300	411/533	12 500	0.01	0.4	0.25	24.80	Toluene
2a	416	31 000	423	3980	0.04	0.4	1.00	24.00	CH^d
2a	425	26 000	508	3800	0.10	0.8	1.25	1130	Toluene
2a	415	15 200	522	4900	0.19	0.8	2.38	10.10	Et$_2$O
2a	425	31 000	558	5600	0.29	1.6	1.81	4.44	THF
2a	436	25 800	593	6100	0.64	2.2	2.91	1.64	CH$_2$Cl$_2$
2a	331	20 600	418/532	6300	0.04	0.4	1.00	24.00	CH$_2$Cl$_2$/H$^+$
2a	425	30 000	600	6900	0.44	2.4	1.83	2.33	Acetone
2a	427	28 600	631	7600	0.47	2.0	2.35	2.65	CH$_3$CN
2a	426	26 400	643	7900	0.09	0.5	1.80	18.20	EtOH
2a	425	27 000	602	6900	0.22	2.4	0.92	3.25	DMSO
2a	430	26 200	617	7100	0.70	2.4	2.92	1.25	DMF
2b	367	35 700	e	e	e	e	e	e	Toluene
3a	383	50 400	410/568	1700	0.24	0.2	12.0	3.80	CH^d
3a	392	30 100	459	3700	0.48	1.3	3.69	4.00	Toluene
3a	383	31 800	464	4600	0.38	2.1	1.81	2.95	Et$_2$O
3a	389	18 200	504	5900	0.76	2.4	3.17	1.00	THF
3a	396	32 200	532	6500	0.56	2.3	2.43	1.91	CH$_2$Cl$_2$
3a	332	7800	e	e	e	e	e	e	CH$_2$Cl$_2$/H$^+$
3a	391	69 800	548	7300	0.09	0.09	1.80	18.20	Acetone
3a	387	27 200	546	7500	0.03	0.03	1.50	1.50	EtOH
3a	390	26 800	533	6900	0.58	0.58	1.93	1.93	DMSO
3a	385	27 800	520	6700	0.27	0.27	1.93	0.93	DMF
3b	321	29 800	400/527	6200	0.01	0.2	0.10	49.50	Toluene

^{a} Relative quantum yield determined in solution using Rhodamine 6G as a reference ($\lambda_{exc} = 488$ nm, $\Phi = 0.88$ in ethanol). ^{b} Stokes shift. ^{c} k_r (10^8 s^{-1}) and k_{nr} (10^8 s^{-1}) were calculated using: $k_r = \Phi_F/\sigma$, $k_{nr} = (1 - \Phi_F)/\sigma$ where σ is the lifetime. ^{d} Cyclohexane. ^{e} Non fluorescent.

lower chelating capacity towards metal or metalloid ions, unless an additional chelating group is introduced in the vicinity.[24] However, there have been reports of some coordination complexes involving SD derivatives. Because SD derivatives have a 6-membered H-bonded ring, they may exhibit weak emission in solution due to the potential of excited-state intramolecular proton transfer (ESIPT) emission.[22,25] The photophysical process known as ESIPT is made up of photo-tautomerism that depends on the location and kind of electronic substitution on the molecular scaffold.[22]

Though the fluorescence of SD is weak,[26] some studies reported SD-made dyes *via* coupling reactions with significant fluorescence. Stoerkler *et al.* synthesized 4-extended SD derivatives **1a–d,** **2a–b,** and **3a–b** starting with 4-bromosalicylaldehyde. Strong naked-eye fluorescence could be induced by substituting certain SD derivatives at the 4-position. Electronic substitution and the kind of π-conjugated spacer affected the optical characteristics of the final dyes. Three distinct spacers (vinyl, ethynyl, or a direct link between SD and different aryl groups) were examined and the emissions were changed according to the π-conjugated spacer (Fig. 1 and Table 1).[22]

4.2 Synthesis of salicylaldehyde

Through a Reimer–Tiemann reaction, SD could be made from phenol and chloroform.[27] By electrolytically reducing salicylic acid on a mercury electrode, SD is produced.[28] The effective conversion of salicylic alcohols to SD under moderate
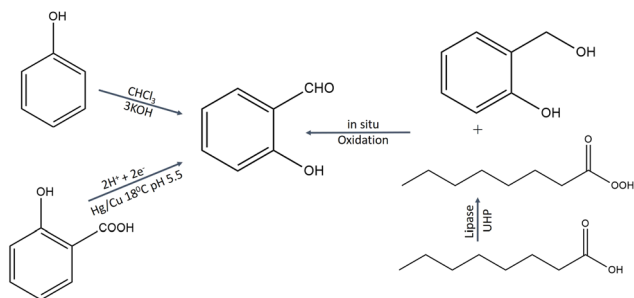
Fig. 2 Synthesis protocol of salicylaldehyde.[27–29]

conditions is facilitated by lipase. High yields (81–95%) of the SD from salicylic alcohol under ideal reaction conditions suggest that the technique has a lot of promise for SD production (Fig. 2).[29]

4.3   Synthesis of salicylaldehyde-capped coinage metal nanoparticles

SD is a hydrophobic organic compound and insoluble in water. That is why it is dissolved in an alkaline solution. In an alkaline solution, SD converted to its phenolate form. However, in the presence of coinage metal ions, the phenolate form of SD was oxidized to the quinone form. On the other hand, coinage metal ions were reduced to zero valent nanoparticles, capped with oxidized SD (OSD).[7,30]

CNPs with OSD capping were prepared under various experimental conditions. Sahu *et al.*[8] synthesized OSD-capped AgNPs at room temperature. Ganguly *et al.* synthesized OSD-capped AgNPs in the presence of UV light for one hour with strong fluorescence. The same group synthesized gold and silver nanoparticles at room temperature with simple aging (without any exposure).[31,32] Sharma *et al.*[7] produced copper nanoparticles from SD after 8 h of simple aging. OSD-capped coinage metal nanoparticles exhibited strong metal-enhanced fluorescence.

OSD-capped CNPs were quite stable. Under ambient conditions, the emission of SD-AgNP hydrosol exhibited a high degree of stability (quantum yield of 7% using quinine sulfate as a reference). After aging for 30 days, the highest emission wavelength of SD-AgNPs was around 419 nm, having previously been approximately 424 nm on day 0. There was only a 9% decrease in fluorescence after 30 days of aging.[8] In comparison to AgNPs, CuNPs were less stable due to the susceptibility of aerial oxidation.[7]

4.4   Generation of metal-enhanced fluorescence (MEF) from salicylaldehyde

SD-passivated CNPs were found to be highly fluorescent exhibiting myriad applications in environmental remediation. SD, being oxidized in its quinone form, maintained a perfect distance from *in situ*-produced CNPs to generate MEF.

Extensive research has been conducted on fluorescence-based biosensor platforms to enhance biosensor performance and sensitivity. Fluorescence signals may be enhanced or
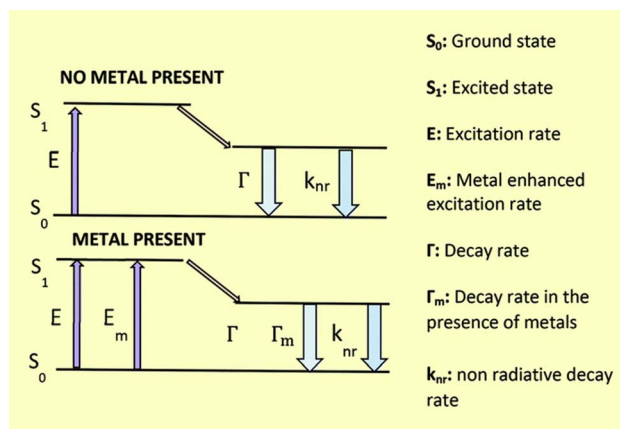

Fig. 3 Energy diagram for fluorescence in the presence and absence of a metal surface. Reproduced with permission from ref. 36, copyright 2024, *Nanoscale*.

quenched in near-optical fields using a variety of structures that make use of metal's properties from the macroscopic to the nanoscopic level. Proximal fluorophores (those in the 5–90 nm range) interact well with metallic surfaces, leading to favorable optical features including shortened fluorophore lifetime, enhanced photostability, and higher quantum yield. The term MEF describes this phenomenon.[9] In 2002, Geddes came up with the term MEF.[33] The excited metal emitted photons, causing MEF. Light interactions with freely movable electrons in a metal particle can increase the incident light field. Such an effect (lightning rod effect) is associated with an extra excitation field with a tremendous effect, causing MEF. Near a silver particle, the local electric field could be multiplied by 140, resulting in a 20 000-fold increase in local intensity and rate of excitation[8,34,35] (Fig. 3).

Fluorophores' quantum efficiency and photostability may both be enhanced by MEF. The free electrons in the metal surface (surface plasmon) pair with the electrons in the fluorophore when it is in close contact with a metallic nanostructure. Here, the metal may be considered an optical antenna that confines concentrated hot areas of electromagnetic radiation in progress. This confinement depends on the metallic nanoparticle's form, composition, and surrounding environment since it is at the particle's surface.[36,37]

Fluorescent materials are often used in biosensing. Much lower quantities of biomarkers utilized in biosensing or bioimaging may be detected with MEF. When exposed to the right wavelength of light, the free surface electrons on metallic nanoparticles (MNPs) resonate. Localized surface plasmon resonance (LSPR) is the name for the charge density oscillations resulting from the metal's electrons being dispersed relative to the particle's core due to this light.[36]

Because each of these factors will alter the electromagnetic field density at the metal nanoparticle surface, the resonance condition depends on the size, shape, distance, and dielectric properties of the metallic nanoparticles and the surrounding medium. It is possible to alter a fluorophore's emission and excitation properties by subjecting it to the near field of

a metallic surface. Because of the fluorophore's increased exposure to the local electric field and the subsequent coupling between it and neighboring MNPs, MEF permits an increase in the excitation rate (Fig. 3).[34,36]

OSD-capped AgNPs aggregated in nature. It was clear from the SEM pictures that the particles were clumped together. The metalized surface was formed by the aggregation of particles measuring around 90 nm, displaying MEF.[8] The oxidized SD was used as a fluorophore and *in situ* produced AgNP, AuNP, and CuNP enhanced fluorescence due to the high photonic mode density associated with the lightning rod effect. After two days of simple aging, the aqueous alkaline solution of SD produced by Ganguly *et al.* showed greatly increased fluorescence at room temperature ($\lambda_{em} \sim 420$ nm, Stokes shift 120 nm, stability >a year), when Ag(I) or Au(III) was added. Such extraordinary fluorescence enhancement caused by Ag and Au particles was attributed to the increased scattering cross-section of the *in situ*-produced aggregated metal particles and the lightning rod effect of the metal aggregates, which concentrated the electric field around the fluorophore (*i.e.*, alkaline solutions of SD).[12,32]

After one hour of UV irradiation, the lifetime of free SD in an alkaline medium was 0.39 nanoseconds. However, the OSD-AgNP hydrosol had a lifetime of 3.85 nanoseconds. The lightning rod effect, which concentrates the electric field surrounding the fluorophore in the presence of Ag^0 owing to LSP, was the reason for the extended fluorescence lifetime in the presence of AgNPs.[31]

4.5 Application of salicylaldehyde-capped coinage metal nanoparticles

4.5.1 Dye removal and recycling. CNPs are also widely used for the elimination of toxic dyes from aqueous systems like magnetic nanoparticles.[38] Sharma *et al.*[39] summarized coinage metal nanoclusters for dye removal, while Padre *et al.*[40] prepared coinage metal-based mono- and bimetallic NPs for catalytic degradation of toxic organic dyes.

Several colors are being investigated for adsorption with nanoparticles. Methyl blue (MB) is the focus of infrequent studies. Rubber, paints, pharmaceuticals, dyes, and varnishes all include MB as a disinfectant.[41] After mixing several dyes with OSD-AgNPs and letting them mature for 20 minutes, no recognizable color change was seen. Only MB produced an immediate blue precipitate, known as MB-Ag^0@$Zn(OH)_2$, with the addition of zinc acetate solution. The supernatant of this precipitate was almost colorless when it formed. Except for Zn^{2+}, no discernible changes occurred when other metal ions (K^+, Al^{3+}, Co^{2+}, Hg^{2+}, Fe^{3+}, Na^+, Ba^{2+}, Pb^{2+}, and Cu^{2+}) were introduced one at a time to the OSD-AgNP hydrocolloid in addition to MB. The blue solid MB-Ag^0@$Zn(OH)_2$ was only formed by Zn^{2+}, suggesting that MB was selectively adsorbed onto Ag^0@$Zn(OH)_2$. The highest possible absorption level was 1065 mg·g^{-1}. To regenerate MB, hot water and ethyl alcohol were applied to the solid MB-Ag^0@$Zn(OH)_2$. But there was insufficient MB regeneration. When deionized water was used to suspend solid MB-Ag^0@$Zn(OH)_2$, and other metal ions were introduced one at a time, only Fe^{3+} produced an instant blue color that indicated MB regeneration. In the presence of Fe^{3+}, around 97% of the MB was recovered. No other metal ion showed a noteworthy MB recovery.[30]

4.5.2 Sensing. The use of nanosensors with recognition sites based on nanoparticles (NPs) plays a crucial role in detecting contaminants. These recognition sites serve a dual purpose by providing indication transduction and selectivity. Three parts make up nanomaterial-enabled sensors: a nanomaterial (or materials), a specificity-enhancing identification element, and a signal transduction mechanism that communicates the analyte's presence. These three divisions can be used to characterize any nanosensor; they are not necessarily unique components inside a sensor. Multiplex detection refers to the ability of sensors to detect more than one analyte. Apart from generating a signal to identify an analyte, "turn-on" or "off/on" sensors were reported.[42]

4.5.2.1 Colorimetric pathway. The unique characteristics of noble metal nanoparticles are referred to as LSPR. The conduction electrons of metal nanoparticles (MNPs) collectively and tenaciously vibrate, when a certain frequency of electromagnetic radiation interacts with them; this resonance is known as LSPR or SPR. MNPs and their surrounding conditions were essential to LSPR. Changes in the size, shape, and composition of the nanoparticles, as well as their sensitivity to the dielectric properties of their surroundings, may be used to adjust the LSPR frequency.[43]

Two kinds of sensors emerge when MNPs interact with the target analyte; one is an aggregation sensor (due to interparticle plasmon coupling of NPs) and another is a refractive index sensor (due to a change in local refractive index – plasmon shift of the medium). This gives rise to the LSPR shift from source frequency. Besides, other classes of sensors also exist, and they are based on Surface Enhanced Raman Spectroscopy (SERS) and MEF. A sensor under focus in the current discussion is an aggregation sensor. Aggregation of MNPs leads to broad and red shifting of the LSPR band. This makes it simple, quick, reliable, and inexpensive to detect the metal ions. The said sensor is called a colorimetric sensor, which detects small molecules, proteins, DNA, pollutants, and noxious metal ions.[44–47]

4.5.2.1.1 H_2O_2 colorimetric sensing. Hydrogen peroxide is widely used in food processing, environmental monitoring, and several chemical sectors due to its strong oxidizing capacity. Furthermore, a variety of biological functions require H_2O_2, a substantial species of reactive oxygen. Imbalanced H_2O_2 concentrations have been linked to Alzheimer's disease, myocardial infarction, and human atherosclerosis.[48–50] H_2O_2 is also considered to be a significant water pollutant. H_2O_2 detection is essential to analytical and biological science. Muralidharan[51] amperometrically sensed H_2O_2 using a glassy carbon electrode infused with copper nanoparticles. Many fluorescence techniques (involving DNA-AgNCs,[50] urea-formaldehyde resin passivated ZnO nanoparticles[52]) were also used. Iridium(III) complex-AgNPs were used as a turn-on fluorescent probe in the presence of H_2O_2.[53] When Sharma *et al.*[7]

introduced H_2O_2 to the alkaline solution of SD, the light-yellow color of SD instantly turned colorless. Then a dark brown color was achieved by adding Cu^{2+} solution. The impact of various competing molecules (Na^+, K^+, Cu^{2+}, Fe^{3+}, Zn^{2+}, fructose, ascorbic acid, and urea) was also investigated. However, only H_2O_2-induced oxidation of SD produced a dark coloration in comparison to other competitive molecules. They experimented with different H_2O_2 concentrations to find the sensor's sensitivity and discovered that colorimetric detection was impossible below 10^{-3} M.[7]

4.5.2.1.2 Fe^{3+} colorimetric sensing. One of the most common transition metals in biological systems is iron. The dual character of iron in biological systems is its vital function in several processes such as electron transport and oxygen metabolism, but it may also be harmful if present in excess. This dichotomy highlights the significance of identifying and regulating the body's iron levels, namely Fe^{3+} ions, to avert related illnesses such as cancer, Parkinson's disease, and Alzheimer's.[8] *N*-Acetyl-L-cysteine,[54] *p*-phenylenediamine,[55] *Poria cocos* extract,[56] and *Sonchus arvensis* leaf extract[57] passivated CNPs were used as a colorimetric sensor for Fe^{3+}.

In the previously discussed paragraph (dye removal and recycling), in the presence of Fe^{3+}, around 97% of MB was recovered. No other metal ion has shown a noteworthy MB recovery. Differences in iron's oxidation states (2/3) and counter anions did not affect the amount of MB recovered. This Fe^{3+} sensing technique used a colorimetric route. From the adsorbed solid MB-Ag^0@$Zn(OH)_2$, iron selectively recovered MB, certifying the ionic iron detecting platform. MB-Ag^0@$Zn(OH)_2$ developed a darker blue color as the concentration of Fe increased. The blue color was visible to the naked eye at iron concentrations between 10^{-2} M and 10^{-7} M, and the absorption spectra revealed that the λ_{max} was 565 nm. Nevertheless, a linear detection range of 10^{-4} M to 10^{-6} M was found, and 10^{-6} M LOD. Other metal ions (Co^{2+}, Cu^{2+}, K^+, Ni^{2+}, Ba^{2+}, Sn^{2+}, Al^{3+}, Na^+, Hg^{2+}, Pb^{2+}), introduced separately with Fe^{3+}, did not alter the restoration of the blue hue, nor did they affect the sensing efficiency.[30]

4.5.2.2 Fluorometric pathway. Light emission is the outcome of the electronic excitation phenomenon during the fluorophore's light absorption process. After light absorption, the fluorophore remains excited, and fluorescence emission is produced with a wavelength longer and energy lower than the excitation wavelength.[58] Fluorophore and ionophore units, which make up fluoroionophores, are used for producing the fluorescence sensor.[33] When constructing a fluorescence sensor, the primary focus should be on two fundamental components: the recognition and signaling units. The former is responsible for the binding's efficiency and selectivity, while the latter transforms the data into an optical signal.[59]

4.5.2.2.1 Ag^+ sensing. Ag ions are regarded as hazardous heavy metals, even though silver compounds are widely used in many sectors (such as electronics, photography, and mirrors). Ag ions accumulate in the body and deactivate sulphydryl enzymes. About 2500 tonnes of silver are discharged into the environment each year as a result of emissions and industrial

wastes; of these, 150 tonnes end up in wastewater sludge and 80 tonnes are combined with surface waters. For the detection of Ag at the trace level in aqueous systems, electrochemical techniques, plasma emission spectroscopy, atomic absorption, and optical tactics have been used.[60–62]

Fluorescence sensing devices for Ag^+ species have been developed in various forms, including small molecules, macromolecules, quantum dots, and nanoparticles.[63] Mehta *et al.*[64] provided an overview of Ag^+ sensing using various current techniques. As an aggregation-induced emission fluorophore, benzoimidazolyl-cyanovinylene (**1**) was developed and a fluorescent peptidyl probe (**2** and **3**) containing this fluorophore was created. The fluorescent peptidyl probes exhibited a ratiometric response to Ag^+ in pure aqueous solutions by preferentially coordinating with Ag^+ among different metal ions.

Gold and silver exhibited the highest fluorescence intensity in the alkaline solution of SD. No other metals show a similar increase in fluorescence. When –CH=O in SD is transformed to –CH=N– (*via* iminic bond formation), gold-enhanced fluorescence was selectively suppressed. Thus, selective and massively amplified silver-enhanced fluorescence was proposed for a sensitive Ag(I) sensor. The LOD was 10×10^{-8} M (far lower than the United States Environmental Protection Agency (EPA) permissible level).[32]

4.5.2.2.2 Fe^{3+} sensing. Fe^{3+} could be detected *via* coinage metal nanoparticles with different methods such as colorimetric and fluorometric. The majority of Fe^{3+} sensing techniques rely on an organic chemosensor that either experiences a "turn-on" process[65] or fluorescence quenching[66] due to the paramagnetic nature of ferric ions. AgNPs were used widely in a fluorometric route for Fe^{3+} sensing. Calix[4]resorcinarene polyhydrazide-capped AgNPs were developed by Makwana *et al.*[67] and exhibited respectable fluorescence. The fluorescence was selectively quenched by Fe^{3+}, and Fe^{3+} sensing was achieved by this approach. A novel Schiff base generated from rhodamine was developed and fluorescence spectroscopy methods were used to detect Fe^{3+}. "Off–on" fluorescence response in semi-aqueous media helped to detect Fe^{3+}.[68]

Fluorescent OSD-AgNPs, synthesized at room temperature, showed quenching in the presence of Fe^{3+}. No other metal ion displayed such kind of quenching. The complexation of the capping agent SD with Fe was ascribed to be the cause of the quenching of silver-enhanced fluorescence. Therefore, iron might be detected with high selectivity and sensitivity using silver-enhanced fluorescence (limit of detection: 2×10^{-9} M).[8,69]

4.5.2.2.3 Cysteine sensing. Cysteine is a common biothiol in biological systems.[70] It is essential for reversible cell redox reactions, including several metabolic and detoxifying biological processes.[70,71] Cysteine has also been shown to be a possible neurotoxin and a biomarker for certain illnesses—inadequate amounts of cysteine cause weakness, edema, skin problems, slow development, and hair depigmentation.[31]

With the aid of binding, the fluorophore emissions may be turned on and off. To recover the fluorescence emission used in

the construction of the fluorescence probe, a particular analyte takes the place of the metal ion ligand.[72,73]

Rajamanikandan used highly fluorescent glutathione decorated copper nanoclusters (GSH-CuNCs) as a fluorescence probe to study a very sensitive and specific detection of L-cysteine (Cys) in human urine samples. With an excitation wavelength of 380 nm, GSH-CuNCs show an emission peak at 613 nm. GSH-CuNCs' emission intensity decreased when Cys was added, indicating that the metal–thiol interaction between the GSH-CuNCs surface and the thiol group containing the Cys analyte may be the cause of the emission intensity quenching.[74]

The OSD-AgNP fluorescence was influenced by the presence of certain amino acids in distinct ways. Tryptophan exhibited increased fluorescence because of its intrinsic fluorescence, whereas cysteine, histidine, and arginine efficiently suppressed fluorescence. Furthermore, the OSD-AgNPs' fluorescence gradually diminished as the cysteine content increased. A strong linear association between $(I_0 - I)/I_0$ and cysteine concentration was found for the concentration range of 0 to 10 mm. The lower detection limit for cysteine was found to be 50 nm. Other amino acids including histidine, arginine, tryptophan, and methionine don't change the OSD-AgNPs' fluorescence. Because of its inherent fluorescence, tryptophan was the only substance in the OSD-AgNPs to exhibit any increased fluorescence. The fluorescence of OSD-AgNPs was selectively quenched by cysteine, and other amino acids did not affect the quenched fluorescence in the OSD-AgNP hydrosol solution caused by cysteine. This phenomenon was explained by changes in the scattering/absorption cross-section and the "lightning rod effect", a change in the electric field density surrounding the fluorophore.[31]

4.5.2.2.4 Cu^{2+} sensing. At high concentrations, copper—a crucial trace element in biological systems—becomes a dangerous and deadly heavy metal.[31] Current advances in emissive sensors for copper, with mechanistic ground and bio-applications, were examined by Li *et al.*[75]

As previously discussed (in the sub-section Cysteine sensing), cysteine was the only amino acid that could specifically quench the fluorescence of OSD-AgNPs. Other amino acids did not quench the fluorescence in the hydrosol solution of OSD-AgNPs (unlike cysteine). Cu^{2+}, a metal ion, could completely restore lost fluorescence. Cu^{2+} ions and cysteine might be detected selectively and sensitively in a single pot using this mechanism of quenching and fluorescence recovery. The off/on fluorescence was caused by changes in the electric field density surrounding the fluorophore and the scattering/absorption cross-section. The restoration of the quenched fluorescence was caused by the formation of Cu(0). The selective quenching and regeneration of fluorescence were largely dependent on the interaction between the fluorophore and the metal ions.[31]

4.5.2.2.5 Pb^{2+} sensing. Although lead poisoning was initially identified as early as 2000 BC, Pb^{2+} is a persistent and highly hazardous environmental pollutant. The Centres for Disease Control (CDC) state that even in the USA, 250 000 children between the ages of one and five have blood lead levels exceeding 10 micrograms per deciliter of blood, which is potentially dangerous.[1–5] Since lead does not degrade, exposure to high levels of lead in children can delay their mental and physical development and result in irreparable brain damage.[76,77]

Pb ion sensing with coinage metal nanoparticles is frequently found in the literature Ganguly *et al.* showed lead, DMSO, and cysteine sensing *via* synergistically evaluating a gold–silver giant cluster.[78,79] Kang *et al.*[80] designed an electrochemical sensing platform of lead ions based on copper, while Anambiga *et al.* designed a colorimetric Pb^{2+} sensor with glutathione-capped silver nanoparticles.[81]

The interaction of Pb^{2+} with the dye molecule MB in the presence of the fluorescent OSD-AgNP hydrosol was the process by which Pb^{2+} turned on fluorescence. MB first quenched the fluorescence of OSD-AgNPs-MB. However, the introduction of Pb^{2+} caused MB to be removed from the vicinity of the silver surface, resulting in the formation of PbS and the release of the quenching action. As a consequence, fluorescence was restored, enabling sensitive and focused Pb^{2+} fluorometric monitoring. The method of turning on the fluorescence was mostly dependent on the interaction of Pb^{2+} with MB and the silver surface.[30] Fluorometric Pb^{2+} sensing (linear detection range: 10^{-5} to 5×10^{-8} M; limit of detection: 5×10^{-8} M) was made possible (Fig. 4). Lead in various natural water sources such as rainfall, tap water, and the Ganga River was measured using the spiking method.[30]

4.5.2.2.6 H_2O_2 sensing. SD itself has weak fluorescence with an emission peak at 500 nm. Adding H_2O_2 increased the overall fluorescence intensity. As the H_2O_2 concentration increased, a new emission peak appeared at 440 nm. The original peak at 500 nm gradually disappeared. A final peak at 420 nm became dominant. The phenolate form was responsible for the weak 500 nm emission. H_2O_2 oxidized the phenolate to the quinone form. The quinone form had a stronger fluorescence with a peak at 420 nm (blue-shifted compared to phenolate). At low H_2O_2 concentrations, only a partial conversion of phenolate to quinone occurred, resulting in a mix of both forms. This explained the initial blue shift (appearance of the 440 nm peak) with some residual 500 nm emission. At high H_2O_2 concentrations, most of the phenolate got converted to quinone, leading to the disappearance of the 500 nm peak and a dominant 420 nm emission.[7] Combination with H_2O_2 and the other competing chemicals (Na^+, K^+, Cu^{2+}, Fe^{3+}, Zn^{2+}, fructose, ascorbic acid, and urea) had negligible effects on the fluorescence of the alkaline SD. This resulted in the selective amplification of fluorescence generated by H_2O_2. The fluorescence amplification effect was not linear in its dependence on H_2O_2 concentration.

H_2O_2 was added gradually in OSD-CuNPs and the effect on the emission was observed. A continuous decrease in fluorescence was noticed with the successive increment of concentration of H_2O_2, without any significant change in λ_{ex} and λ_{em} (a linear detection was obtained in the range of 10^{-4} M to 10^{-6} M with a limit of detection of 10^{-6} M). The primary cause of
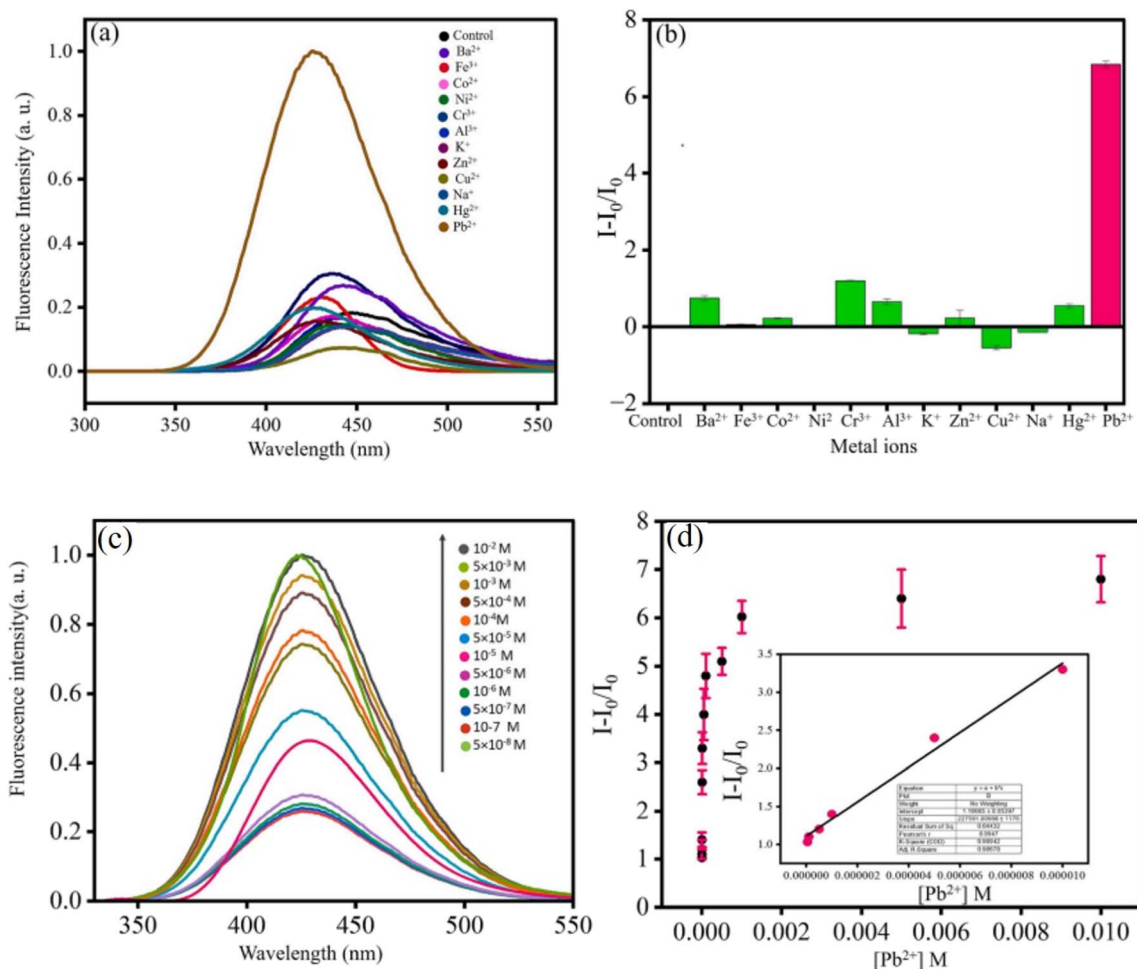
Fig. 4 Effect of metal ions on (OSD-AgNPs-MB); (a) fluorescence spectra and (b) bar diagram; (c) fluorescence spectra of OSD-AgNPs-MB at different [Pb^{2+}] and (d) plot of I/I_0 vs. [Pb^{2+}] and linear detection range of Pb^{2+} detection. Reproduced with permission from ref. 30, copyright 2024, Spectrochim. Acta, Part A.

fluorescence quenching was the oxidation of Cu^0 by H$_2$O$_2$, destroying MEF in the absence of a metal surface.[7]

4.5.3 H$_2$O$_2$ removal and absorption. To validate the quenching of OSD-CuNP hydrosol's fluorescence caused by H$_2$O$_2$, Sharma et al.[7] used two cotton wools. While one cotton wool was left untreated, the other cotton wool was impregnated with CuNPs by soaking it in CuNPs. Two distinct glass funnels were fitted with both cotton wools. One by one, H$_2$O$_2$ was run through each funnel. After being removed from the funnel, the filtrate was added to the alkaline SD. A significant increase in the fluorescence from the untreated H$_2$O$_2$ filtrate was observed. Conversely, the cotton wool filtrate treated with CuNPs showed little enhancement of fluorescence. These findings supported the first use of CuNPs in sensing, wherein H$_2$O$_2$ increased SD's fluorescence. Because untreated cotton wool was unable to absorb H$_2$O$_2$, the concentration of the original H$_2$O$_2$ and filtered H$_2$O$_2$ was almost the same. Actually, after passing through the treated cotton wool, the concentration of H$_2$O$_2$ was low enough that there was hardly any noticeable fluorescence amplification (λ_{ex} = 290 nm). The filtrate from treated cotton wool had an H$_2$O$_2$ concentration that was eleven times lower than that of the

untreated cotton wool. Though the untreated cotton wool absorbed some H$_2$O$_2$, the concentration of H$_2$O$_2$ did not change since there was no chemical interaction between the cotton wool and H$_2$O$_2$ in the experimental setup (Fig. 5).

4.5.4 Imine-induced selectivity of silver and gold nanoparticles. As mentioned above, in situ-produced Ag and Au particles were reported to cause a remarkable fluorescence increase in the alkaline solutions of SD. However, imine bond formation in the presence of ammonia or primary amines resulted in the quantitative elimination of Au-enhanced fluorescence, while the OSD-AgNP hydrosol did not show any remarkable fluorescence loss.[32] Imine brought selectivity for silver-enhanced fluorescence. The amine group, possibly as a result of the production of lossy surface waves surrounding the gold nanoparticles, produced a particular wave vector matching that which increased silver-enhanced fluorescence while reducing gold-enhanced fluorescence (Fig. 6).[32]

4.5.5 Fate of salicylaldehyde-capped coinage metal nanoparticles. OSD-AgNPs often have a prominent surface plasmon band in the visible spectrum, while silver hydrosol typically has a yellow hue with an absorption λ_{max} in the absorption spectra
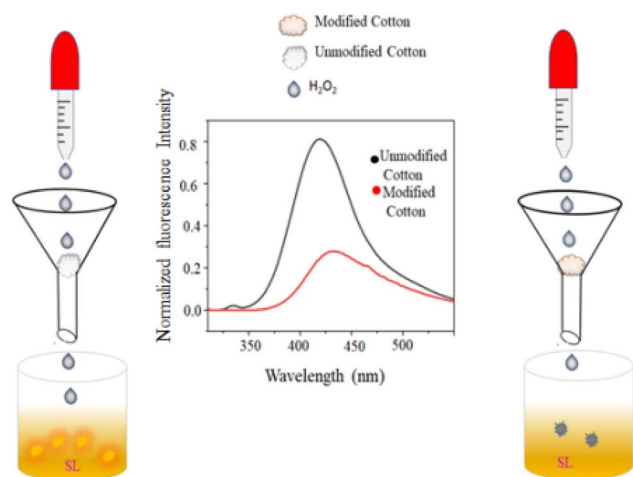
Fig. 5 H$_2$O$_2$ removal using OSD-CuNP-modified cotton wool.[7] Reproduced with permission from ref. 7, copyright 2024, *New J. Chem.*

Fig. 7 TEM and HRTEM digital images of CuNPs. Reproduced with permission from ref. 7, copyright 2024, *New J. Chem.*

between 390 and 400 nm. In the case of OSD-AgNPs, the reducing agent (phenolate form of SD) and stabilizing agent (quinone form of SD) were yellow. Because of the protective ligand and AgNP surface plasmon's overlapping band, OSD-AgNPs showed a large peak at around 400 nm.[8]

The absorption spectra of the yellow-colored alkaline SD solution showed two peaks at 330 and 373 nm, which were attributed to the phenolate and quinone forms. The quinone form (λ_{max} 381 nm) was the only form found in OSD-CuNPs, whereas the phenolate form (λ_{max} 330 nm) entirely disappeared. OSD-CuNP formation significantly reduced the absorbance at 381 nm (Table 2).
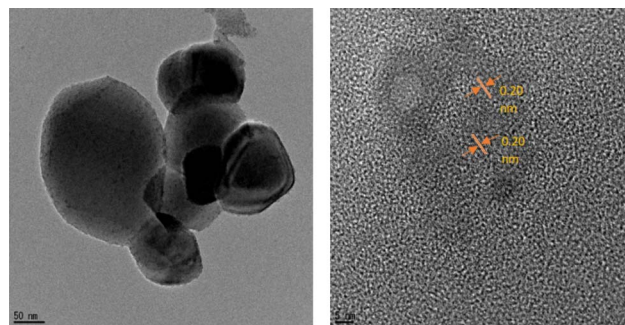
The values of 2θ at 38°, 44°, 64°, and 77° correspond to (111), (200), (220), and (311) for zero-valent Ag in OSD-AgNPs, respectively.[8] The TEM image reflected an aggregated structure, while the HR-TEM image indicated a zero valent lattice fringe (Fig. 7).

XPS and lattice fringes both show that Ag is in the zero-oxidation state. The (111) plane of Ag^0 was indicated by a fringe spacing of 0.236 nm. Binding energies of 365.81 and 371.82 eV corresponded to Ag^0 3d$_{5/2}$ and Ag^0 3d$_{3/2}$ respectively.[31]

4.5.6 Effect of the components of salicylaldehyde. With Ag$^+$ or Au^{3+} ions, there is no metal-enhanced fluorescence effect seen with benzaldehyde or phenol. This metal-enhanced fluorescence is made possible by SD's unique structure, namely the presence of the hydroxyl group (OH) at position 2 on the benzene ring. This heightened impact is probably caused by the aging process making it easier for the metal ions and SD molecules to form aggregates.[32]
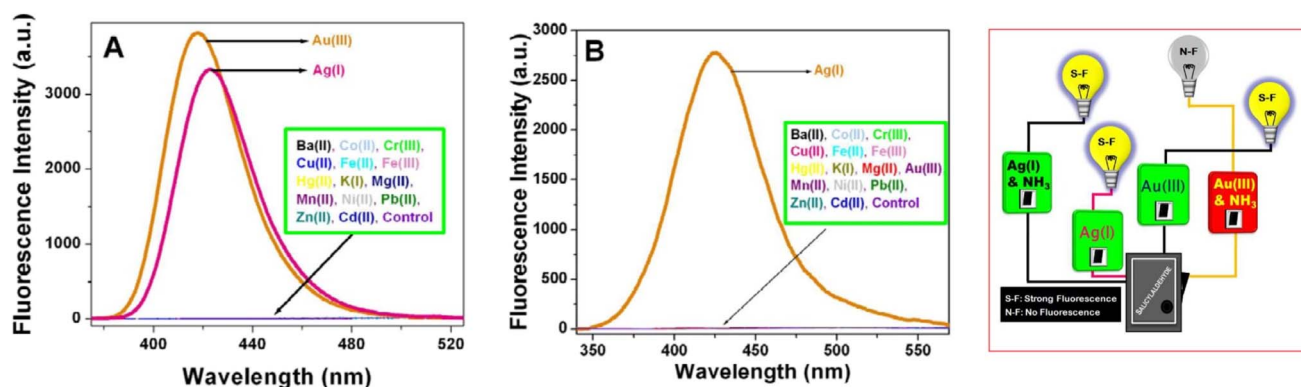

Fig. 6 Displayed imine brings selectivity for silver–enhanced fluorescence (A) without imminic bond, (B) with imminic bonds. Reproduced with permission from ref. 32, copyright 2024, *Dalton Trans.*

Table 2 Synthetic conditions and properties of salicylaldehyde capped coinage metal nanoparticles

Salicylaldehyde-capped nanoparticles	Synthesis conditions	λ_{ex} and λ_{em} (nm)	Size (nm)	Shape	Oxidation state	Lattice spacing (nm)
AgNPs[8]	Room temperature	290 and 424	90	Aggregated	Zero	0.232
AgNPs[31]	UV light	290 and 424	—	Aggregated	Zero	0.236
CuNPs[7]	Room temperature	290 and 420	—	Aggregated	Zero	0.20

5. Mono-iminic Schiff base

Schiff bases resemble aldehyde or ketone derivatives but have an imine or azomethine group instead of the carbonyl group.[82] First described by Hugo Schiff in 1864, Schiff bases are adaptable ligands produced by condensing an amino molecule with carbonyl compounds.[83,84] Schiff bases are often formed by heat, acid or base catalysis, or both. The crystalline solids that are the typical Schiff bases are weakly basic, but some may also form insoluble salts with strong acids.[84] Usually, a condensation reaction between an aldehyde or ketone (also called the carbonyl component) and a primary or secondary amine produces Schiff bases. A carbon–nitrogen double bond, which is the defining property of Schiff bases, is formed during the condensation reaction due to the amine group's nucleophilic assault on the carbonyl carbon of the aldehyde or ketone. R1(C=N)R2, where R1 and R2 are organic groups, can be used to illustrate the overall structure of a Schiff base. One important structural component is the double bond between carbon and nitrogen in the center. Schiff bases can have several isomeric configurations, such as E/Z isomers, contingent on the configuration of substituents surrounding the carbon–nitrogen double bond.[85] Schiff bases are susceptible to tautomerism, a phenomenon in which the nitrogen's hydrogen atom migrates to the carbon atom, producing distinct structural isomers.[86]

Schiff bases are frequently employed in nanoparticle production. These substances are adaptable and can function as stabilizing agents or ligands throughout the nanoparticle manufacturing process.[87] Schiff bases are frequently used in the formation of nanoparticles because of their capacity to chelate metal ions. Metal nanoparticle production and stabilization are aided by this chelation process. Metal ions and the Schiff base may coordinate, resulting in the reduction and nucleation of metal nanoparticles. Schiff bases can also function as capping or reducing agents, which can affect the stability, size, and form of the resultant nanoparticles.[88] Applications for synthesizing nanoparticles with Schiff bases include drug delivery, sensing, catalysis, and other areas of nanotechnology. Scholars frequently investigate various Schiff bases and their metal complexes to customize the characteristics of nanoparticles for certain uses.[88]

5.1 Synthesis of salicylaldehyde-derived mono-iminic Schiff bases

Ample Schiff bases are synthesized *via* condensation reaction with amines. Fig. 8 displays schematic representations of mono-iminic Schiff bases, reported for passivating CNPs.

5.2 Design of mono-iminic Schiff base capping on CNPs

5.2.1 Capping *via* replacement reaction. Jimoh et al.[89] reported the synthesis of a thiolated Schiff base ligand by the reaction of SD and 4-amino thiophenol, followed by its subsequent anchoring onto the surface of fluorescent AuNPs through replacing citrate as a stabilizing agent. Kannaiyan et al.[90] synthesized AgNPs using starch and modified them with anionic dye (acid fuchsin) and aldehyde (SD and cinnamaldehyde). Almashal et al. synthesized a Schiff base (from the condensation reaction of SD and 2-aminobenzoic acid) as a capping agent for the synthesis of AgNPs by preventing the overgrowth of AgO (Fig. 9 and Table 3).[91]

5.2.2 Enol keto tautomerism. Mahmoodi et al.[94] synthesized salicylidene-aniline (anil) photochromes with thiol groups (thiolated Schiff bases), and their photochromic characteristics were reported. AgNP surfaces showed a bathochromic shift in the absorption band and a photochromic response associated with the light-induced tautomerization of the anil functionality (Fig. 9).

5.2.3 Quinone formation. Sharma et al.[92] synthesized silver and copper hydrosols by employing emissive semi-carbazone (SC), a Schiff base made from semicarbazide and SD. SD reduced ionic coinage metal salt to zero-valent metal nanoparticles and SD was oxidized to the quinone form. Cu[0] nanoparticles are susceptible to aerial oxidation and converted to
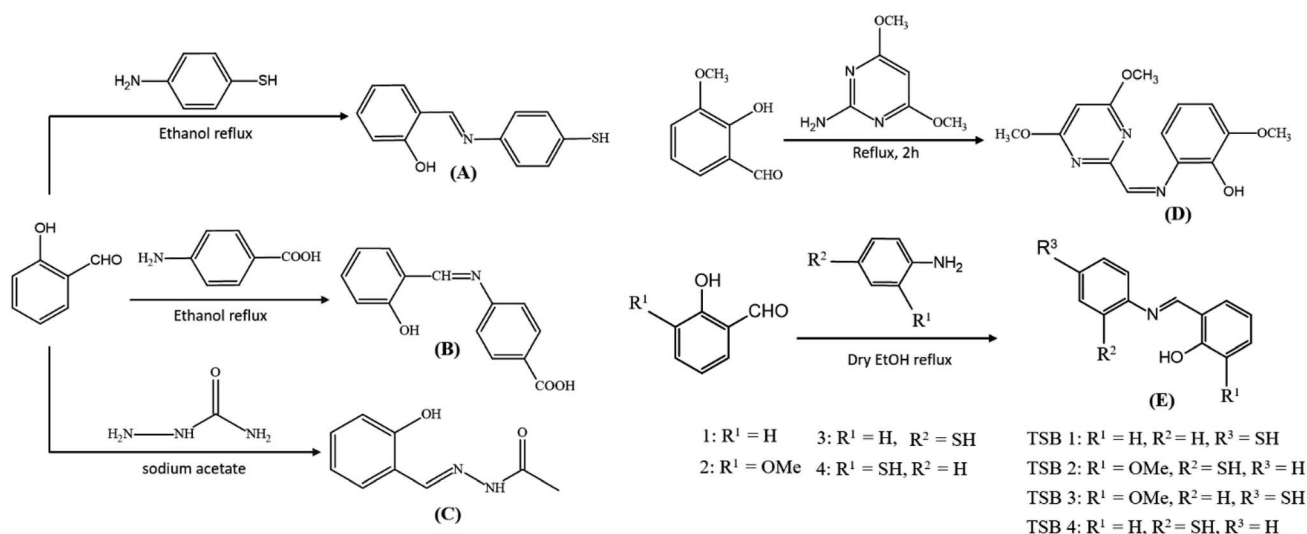

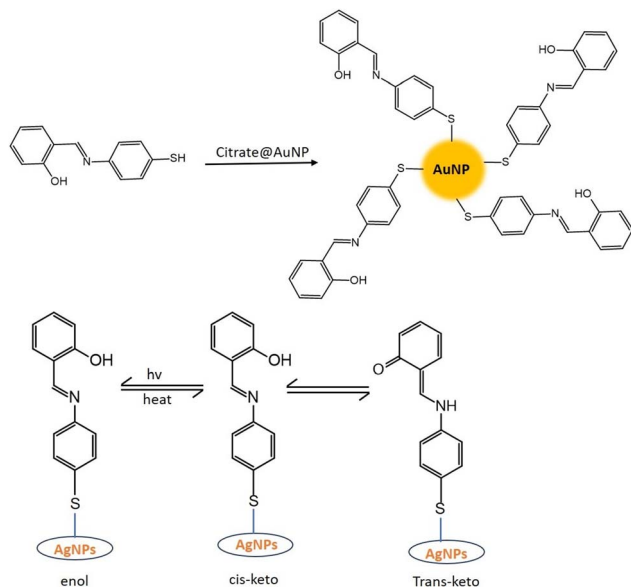Fig. 8   Schematic representation for the synthesis of SD-derived Schiff bases.

Fig. 9 Mono-iminic Schiff base capping on coinage metal nano-particle synthesis mechanism.

copper oxide after a short period. The quinone (oxidized) form of semi-carbazone acted as a stabilizing agent for nanoparticles.

5.3 Manipulation of metal-enhanced fluorescence

Sharma *et al.*[92] reported MEF involving SC (a mono-iminic Schiff base). Through a sequence of redox reactions and energy transfer processes, the interaction between CuO and Ag nanoparticles in an alkaline SC solution could result in significant MEF. Cu^{2+} ions first formed chelates in an alkaline SC solution, which quenched the fluorescence of SC. Electrons go from a full orbital in the ligand to an empty orbital in the metal centers as a result of ligand-to-metal charge transfer, or LMCT, which causes this quenching. High-valent metal centers like Cu(II), which contain low-energy empty d orbitals appropriate for LMCT, are commonly involved in this transition. Because electron-rich ligands (such as halides and carboxylates) make it easier for electrons to transfer to the metal, LMCT states are more likely to occur. This bond dissociation causes non-radiative decay processes.

Cu^{2+} ions were reduced to Cu^0 and then oxidized to generate CuO nanoparticles over an 8 hour aging period. At the same time, SC oxidized to quinone (OSC). Fluorescence quenching was caused by energy trapping between the fluorophore (OSC) and CuO nanoparticles upon excitation with 290 nm photons. Heat energy, which was not radiative, was created from this stored energy. This quenching was facilitated by the "lossy surface waves" phenomena that Lakowicz described.[96] Owing to a mismatch in the wavevector, generated electron oscillations could not radiate effectively, giving rise to these waves. Ag^0 nanoparticles were developed in the CuO-OSC system when Ag^+ was added. Cu^0 and CuO were also formed. Due to the lightning rod effect, the Ag^0 nanoparticles, which had plasmon bands, released the energy that was previously held at 420 nm, greatly increasing the fluorescence. As a result, the quantum yield increased to 6.5% as compared to quinine sulfate. Strong MEF was produced when Cu and Ag nanoparticles were present together because they efficiently transmitted energy from the fluorophore to the metallic nanoparticles. This system's heightened fluorescence was a result of the synergy between Ag and CuO nanoparticles (Fig. 10).[92]

5.4 Applications of salicylaldehyde derived mono-iminic Schiff base capped coinage metal nanoparticles

5.4.1 Sensing

5.4.1.1 Colorimetric pathway

Table 3 Synthesis and properties of salicylaldehyde-derived Schiff base capped CNPs

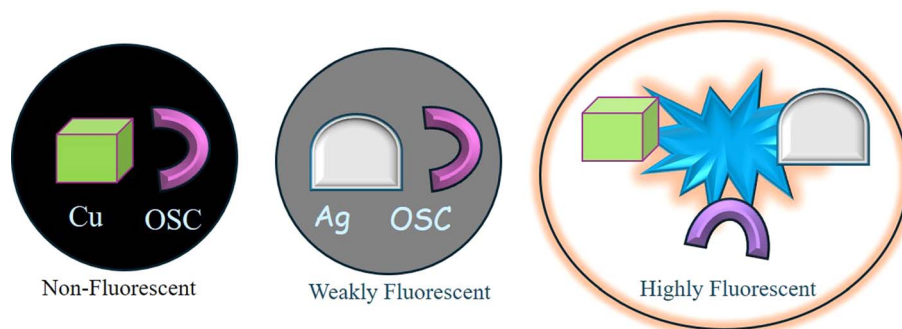| Capping agent	Reducing agent	Salt precursor	Conditions	NPs	Shape	Size (nm)
Thiolated Schiff base ligand[89] (A)	Trisodium citrate	$HAuCl_4 \cdot 3H_2O$	Room temperature	AuNPs	Spherical	8–10
4-((2-Hydroxybenzylidene) amino) benzoic acid[91] (B)	Maltose sugar	$AgNO_3$	60 °C	AgNPs	Spherical	6–45
Semi-carbazone oxidized form (C)[92]	Semi-carbazone	$AgNO_3$ + $CuSO_4$	Aged for 8 h	Ag–Cu hydrosol	Aggregated spheroid	~30
2-((4,6-Dimethoxypyrimidine-2-yl) methyleneenamino)-6-methoxyphenol (DPMM)[93] (D)	$NaBH_4$	$HAuCl_4 \cdot 3H_2O$	Modified Brust–Schiffrin method	AuNPs	Granular	38.14 ± 4.5
2-(((4-Mercaptophenyl)imino)methyl) phenol (TSB 1)[94] (E)	$NaBH_4$	$AgNO_3$	Room temperature with N_2 gas	AgNPs	Spherical	<40
2-(((2-Mercaptophenyl)imino)methyl)-6-methoxyphenol (TSB 2)[94] (E)	$NaBH_4$	$AgNO_3$	Ice bath with N_2 gas	AgNPs	—	—
2-(((4-Mercaptophenyl)imino)methyl)-6-methoxyphenol (TSB 3)[94] (E)	$NaBH_4$	$AgNO_3$	Room temperature with N_2 gas	AgNPs	—	—
2-(((2-Mercaptophenyl)imino)methyl) phenol (TSB 4)[94] (E)	$NaBH_4$	$AgNO_3$	Ice bath with N_2 gas	AgNPs	—	—
Cinnamaldehyde[90] (F)	Starch	$AgNO_3$	60 °C, pH 13	AgNPs	Spherical	5–10
Chitosan-SD Schiff base[95] (G)	Chitosan-SD Schiff base	$AgNO_3$	60 °C with magnetic stirring continued for 12 h	AgNPs	Spherical	5 to 20 nm

Fig. 10 Synergism of Cu and Ag to generate strong metal-enhanced fluorescence.[92] Reproduced with permission from ref. 92, copyright 2024, *Appl. Nanosci.*

5.4.1.1.1 Ag^+ sensing. The addition of Ag^+ to a solution of SC caused a visible color change, along with the formation of AgNPs. At a high concentration of Ag^+ (10^{-2} M), the yellow color of SC turned white with the formation of a precipitate. At a lower concentration of Ag^+ (10^{-3} M), the solution turned a distinct red color. Other metal ions tested (Na^+, K^+, Pb^{2+}, Hg^{2+}, Zn^{2+}, Cu^{2+}, Fe^{3+}, Ba^{2+}, Cd^{2+}, Co^{3+}, Al^{3+}) at the same concentration (10^{-3} M) did not cause any significant color change. This indicated good selectivity of SC for Ag^+ detection. The red color arose from two factors. The plasmonic band of AgNPs formed by the interaction of Ag^+ and SC exhibited a specific light absorption pattern called the plasmonic band. This band typically appears in the red region for aggregated AgNPs. Aggregation of AgNPs in the presence of SC further intensified the red color in the plasmonic band.[92]

5.4.1.2 Fluorometric pathway

5.4.1.2.1 Fe^{3+} sensing. Emissive Schiff base ligand-capped AuNPs showed quenching in the presence of Fe^{3+}. No other metal ions (Al^{3+}, Ni^{2+}, Cu^{2+}, Co^{2+}, Hg^{2+}, Zn^{2+}, Na^+, K^+, Ca^{2+}, and Rb^+) showed such type of quenching. The quenching was attributed to chelation-enhanced quenching because Fe^{3+} is paramagnetic. Because Fe^{3+} has a strong thermodynamic affinity for phenolic-C=N and –OH groups—a combination of the oxygen of the phenol ring and the imino nitrogen of the amine—the AuNP chemosensor showed selectivity for Fe^{3+} ions. The great propensity of phenol to deprotonate during complex formation resulted in the development of this hybrid, which had quick metal-to-ligand binding kinetics, not achievable with other transition-metal ions. For Fe^{3+}, the AuNP estimated detection limit was 1.2 μM, and the fluorescence turn-on method outperformed the switch-off method. Furthermore, a 1 : 1 binding mode for Fe^{3+} was shown by the absorption and emission spectrum analyses, with robust binding constants of 2.9×10^5 M^{-1} and 8.5×10^5 M^{-1}, respectively. The AuNP chemosensor had a high selectivity for Fe^{3+} ions, which made it useful for detecting Fe^{3+} in a variety of applications, particularly fluorescence sensing.[89]

5.4.1.2.2 Ag^+ and Cu^{2+} dual sensing. (E)-1-((Pyridin-4-yl)methylene),[97] 1-(4-(pyridine-4-yl)benzylidene)thiosemicarbazide,[98] and L-cysteine capped CdTe quantum dots[99] were used for the fluorimetric and/or colorimetric sensing of silver and copper simultaneously.

Cu^{2+} showed quenching in the presence of emissive SC (a Schiff base synthesized from semicarbazide and SD) due to the formation of copper oxide nanoparticles *in situ*. With a limit of detection of 13 μM, this chemical showed a linear detection range from 10^{-4} to 5×10^{-8} M. Copper oxide nanoparticles were formed as a result of the complexation–reduction technique, used to achieve the detection. Moreover, the addition of Ag^+ ions to the solution produced Ag^0 and Cu^0 nanoparticles, which had a much higher fluorescence. This made it possible to detect Ag^+ ions with a linear detection range of 10^{-3} to 10^{-7} M and a detection limit of 7.7 μM. This made the detection of Ag^+ ions sensitive and selective. Using turn-on/off fluorescence, the study showed how to detect Cu^{2+} and Ag^+ ions simultaneously in a single reaction vessel.[92]

5.4.2 Antibacterial activity. The growing prevalence of antibiotic resistance in bacteria is becoming a significant issue for accurate infectious illness diagnosis and treatment. Significant advancements in the formation of medications based on nanotechnology have been made in recent decades to address the issue of multidrug resistance in bacteria. Because of its strong and broad-spectrum antibacterial qualities, Ag, Cu, and Au are among those that show the most promise in tackling this problem.[100,101]

Ganguly *et al.* reported[102] the antibacterial activity of gold core–silver shell giant nanoclusters, applied to form antibacterial cotton and papers. Al-Hakkani[103] reviewed the antibacterial activity of copper-based nanoparticles. Tang and Zheng[100] and Mobed[104] also reviewed antibacterial activity from silver and gold nanoparticles. Here we concentrated on the antibacterial activity of coinage metal nanoparticles passivated with SD.

Antibacterial and antioxidant studies of DPMM indicated that DPMM-AuNPs were more active than DPMM. *In vitro*, anticancer results showed that the DPMM-AuNPs had significant cytotoxic activity against cancer cell lines and the least toxic effect on the normal cell line.[93] AgNPs were tested against *S. aureus*, *P. aeruginosa*, *K. pneumoniae*, and *E. coli* and found to have significant inhibitory activity against these bacteria species (Fig. 11).[91]
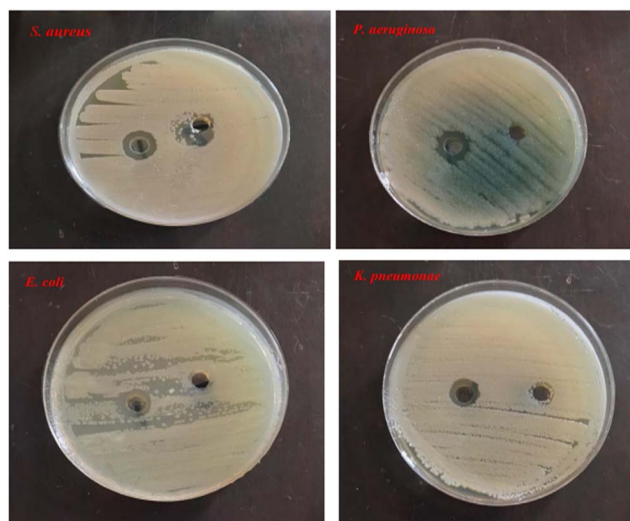
Fig. 11 Schiff base capped AgNPs displayed antibacterial activity against *S. aureus*, *P. aeruginosa*, *K. pneumoniae*, and *E. coli*.[91] Reproduced with permission from ref. 91, copyright 2024, *Egypt. J. Chem.*

5.5 Fate of coinage metals, passivated with salicylaldehyde-derived monoiminic Schiff bases

SD-derived Schiff base (A) capped AuNPs existed in a zero-oxidation state. The peaks in the XRD pattern at $2\theta = 38.2$, 44.4, 64.5, 77.5, and 81.7° were the same as those documented in the literature and correlated to the (111), (200), (220), (311), and (222) planes in the AuNPs. The TEM image displayed spherical particles that were evenly dispersed and had an average diameter of 8–10 nm.[89] TEM analysis results show that the particle size of the DPMM-AuNPs was found to be approximately 38.14 ± 4.5 nm.[93]

Semicarbazide and SD were condensed to produce SC, an imine derivative. SC's FTIR spectrum was captured. The O–H bond's symmetric and asymmetric stretching vibrations were represented by the band at 3168 cm^{-1}. The existence of a band at 1696 cm^{-1} suggested that the C=O bond had several bending vibration modes. Different modes of the N–H bond were indicated by the existence of a band at 3478 cm^{-1}.

Cu and Ag were clearly in a zero oxidation state in CuSCAg[92] based on the XPS spectrum. Cu's zero oxidation state was confirmed by the binding energies of Cu, which were 932.56 eV and 962.40 eV, respectively, with Cu $2p_{3/2}$ and Cu $2p_{5/2}$. In the zero oxidation state, Ag binding energies of 374.15 eV and 368.12 eV were confirmed by Ag $3d_{3/2}$ and Ag $3d_{5/2}$, respectively. Nonetheless, zero-valent silver and CuO were detected in the XRD pattern. Surface oxidation of zero-valent copper in CuO-SCAg was most likely detected by X-ray radiation. The 2θ values for CuO nanoparticles were 32.36°, 35.42°, 38.1°, 48.82°, and 61.52°, representing (110), (111), (200), (202), and (311), respectively; for Ag^0 in the CuOSCAg hydrosol, the 2θ values were 38.12°, 44.18°, 64.46°, and 77.42°.[92]

6. Diiminic Schiff base (DSB)

DSB, such as salen and salen-like compounds, are derived from diamines and SD. These days, a lot of emphasis is focused on the chemistry of salen due to its many uses. Nowadays, "salen" is a sophisticated term in synthetic chemistry. It's been a long trip since Pfeiffer first reported "salen" in 1933. Salen and its derivatives have been widely used in synthetic, analytical, and biological chemistry.[19]

Condensation products of SD and different diamines constitute an important class of diiminic Schiff bases (DSBs). This class of compounds has been rediscovered as reducing as well as capping agents. Two iminic bonds (>C=N–) are present in the DSB. DSBs are the result of a condensation process involving one diamine and two SD molecules. A process when a small molecule, such as water or methanol, is lost at the same time that two or more molecules join to produce a larger molecule is called a condensation reaction. Salen is produced by condensing SD and ethylenediamine. It has been demonstrated that these salen-like molecules are an excellent candidate for coinage metal-enhanced fluorescence.[12,105] Different DSBs were formed by adjusting the diamines, or the distance between two imines while maintaining a constant aldehyde. Variable spacers were present in these DSBs between two iminic linkages. Six distinct DSBs were made from SD and various diamines.[12,105]

6.1 Salicylaldehyde-derived diiminic Schiff bases for the evaluation of coinage metal nanoparticles

DSB compounds were insoluble and dissolved in an alkaline aqueous solution. HAuClO$_4$, AgNO$_3$, and CuSO$_4$ were introduced individually under different experimental conditions under UV light (365 nm) exposure in the alkaline aqueous medium of DSB. As a result, pale yellow-colored copper nanoparticles, wine-red colored gold nanoparticles, and yellowish-brown colored silver nanoparticles were produced.[12,106] DSBs were utilized to stabilize nanoparticles.

Different diamines and SD were used to create different Schiff bases. Triethylenetetramine was condensed with SD to form another Schiff base. The Schiff base and the appropriate metal salts were used to form coinage metal nanoparticles (Cu, Ag, and Au) in an aqueous alkaline solution. AgNPs and AuNPs did not require UV light to be developed, while CuNPs did. During the production of the nanoparticles, the Schiff base underwent oxidation to produce an oxidized condensation product (OCP), which served as a fluorophore and stabilizer for the nanoparticles.

The DSB family of compounds was found to be effectively capping and reducing agents under UV light. Ethylenediamine was used in the synthesis of C1, or salen. Similarly, 1,3-propylenediamine, 1,4-butanediamine, *o*-phenylenediamine, *m*-phenylenediamine, and *p*-phenylenediamine were used in place of ethylenediamine to produce C2 (salprn), C3 (salben), C4, C5, and C6. To form the Schiff base C1 (salen), ethylenediamine and methanolic SD react with condensation. Using other diamines, identical steps were taken to produce the additional Schiff bases (C2 to C6).[19] AgNO$_3$ in an alkaline solution oxidized the DSB to produce stable Ag^0 at room temperature under 1 h of 365 nm UV light. At λ_{em} of 412 nm, the solution displayed strong AgNP enhanced fluorescence with an emission wavelength.[105–107] Ionic
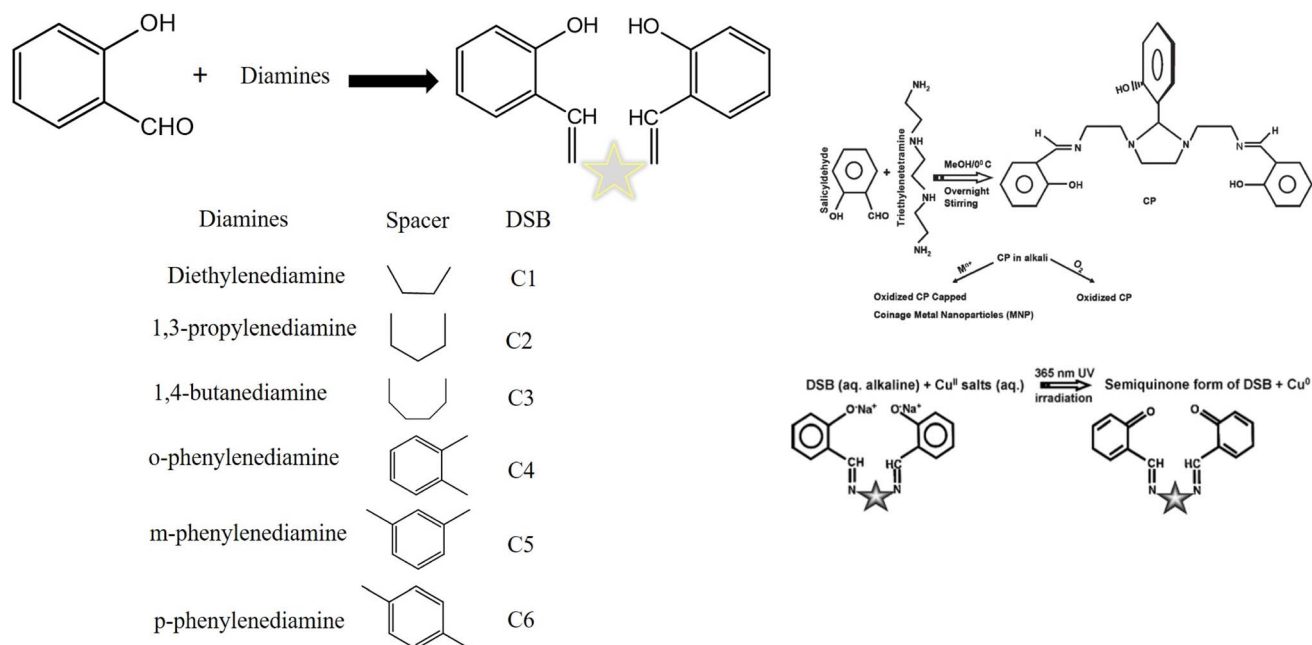
Fig. 12 Distinct diamines and salicylaldehyde-derived synthetic DSBs[105] and the mechanism of the formation of metal nanoparticles.[19]

copper salt in an alkaline solution oxidized the DSB to produce stable Cu^0 at room temperature under 9 h of 365 nm UV light. At λ_{em} of 429 nm, the solution displayed strong CuNP enhanced fluorescence with an emission wavelength (Fig. 12).[105]

6.2 Manipulation of metal-enhanced fluorescence

The type of spacer between the two iminic bonds in the DSB affected the fluorescence behavior of the CNPs. It was discovered that DSBs had a great candidacy for MEF. Because they were hydrophobic organic molecules, DSBs were insoluble in water. *In situ* generated metal nanoparticles with oxidized DSB as the fluorophore showed interesting fluorescence behavior. The metals and spacer were required for both quenching and amplification of the fluorescence. For this reason, such MEF was utilized to identify chemical molecules and environmentally hazardous metal ions.[12]

In the case of DSB-capped AuNP fluorescence behavior,[19] a radiation-free transfer of the fluorophore's excitation energy to the quencher molecule was observed. While the photoexcited electrons of the quinones returned to the ground state, the electrons of the quencher Au^0 went to a higher energy state. The Au^0 molecule lost its obtained energy when it equilibrated with the solvent. Plotting the I_0/I, where I_0 is the fluorescence intensity of the free DSB following irradiation and I is the fluorescence intensity of the exposed DSB with varying Au^0 concentrations, Stern–Volmer graphs depicted both the static and dynamic quenching. Compared to C2, the slope of these plots for C5 is steeper. It suggested a stronger interaction between quencher Au^0 and C5. Compared to C2, the bigger size of C5 stabilized AuNPs had a lower surface area (or surface-to-volume ratio). For the latter, there should be a greater quenching magnitude. The observable fact, however, was the

opposite. The two structures' stiffness was most likely the cause of this occurrence. C5 was not as flexible as C2. It was the presence of a *meta*-substituted phenyl ring that stopped free rotation between the C5's two iminic bonds. Conversely, the aliphatic chain that stretches between two iminic bonds is in charge of assuming different rotameric conformations, which resulted in reduced fluorophore contact with AuNPs. There was a strong correlation between the fluorescence intensity of the capping agent and the size of the nanoparticles. The surfaces of homogeneous colloids were not as useful for MEF as aggregates, according to Lakowicz *et al.*[108] As a result, photoproduced AuNPs with a narrow size distribution quenched fluorescence by reducing the fluorophore's dipole oscillations.

On the other hand, DSB-capped AgNPs exhibited intriguing fluorescence behaviors. The "lightning rod effect" was responsible for the silver colloids' remarkable enhancement of fluorescence.[109] AgNPs improved the rate of excitation by concentrating the local field on the fluorophore. The inherent radiative decay rate of a fluorophore, or how quickly it emits photons, may likewise be altered by the silver metal. Radiative decay engineering (RDE) is the process of linking the molecular dipole of the fluorophore with the metal's surface plasmon band to increase the rate of radiative decay and produce a higher quantum yield fluorescence emission. The capping agent's fluorescence intensity and the size of the NPs are highly correlated.[110]

When compared to just exposed DSB, exposed DSB solutions with *in situ* photoproduced AgNPs exhibited a significantly different fluorescence characteristic. Except for C5, all of the DSBs exhibited a sudden rise in fluorescence intensity after being exposed to silver nitrate for three hours. The intensity of fluorescence was enhanced to varying degrees by various DSBs. Fluorescence damping only happened for C5. AgNPs maximally

increased the fluorescence intensity for C3. In this context, it was also clear that the amplification of fluorescence is noticeably modest and that, occasionally, quenching (C5) of fluorescence is also observed when two iminic bonds are separated by an aromatic group. DSBs are a novel class of fluorophores that exhibit metal-enhanced fluorescence in an alkaline aqueous solution. For the extreme variation in fluorescence behavior, the distance between the metal nanoparticles and the capping agent, or fluorophore, may be crucial. Nearby, metallic surfaces greatly damped fluorophore emission up to ∼50 Å. The probe experienced maximum enhancement at a distance of around 100 Å from the metallic surface. Sokolov *et al.*[111] found that the quenching zone of the fluorophore (capping agent) occurs at a distance of approximately 600 Å. AuNPs are more likely to remain closer, while larger AgNPs are at a suitable distance from their capping agent, exhibiting enhanced fluorescence.

When the DSB was exposed to UV radiation in the presence of copper salt, the fluorescence (λ_{em} 429 nm) of each exposed reaction mixture, for example, C1, C2, C3, and C4, was dramatically increased, because *in situ* Cu[0] was produced. Remarkably, the quenching phenomena were noted for C5 and C6. An enormous increase in emission intensity was seen when aliphatic groups (C1–C3) were present between the two iminic bonds. In contrast, when photoproduced Cu[0] was present, an aromatic group positioned between the two iminic bonds showed a slight increase in fluorescence (C4) and occasionally quenching (C5 and C6). Thus, in the presence of CuNPs, generated *in situ* in the reaction mixture as a result of UV light irradiation, the spacer between the iminic bonds significantly tuned the fluorescence behavior of the exposed DSBs. This illustrated the extent of varying MEF in the presence of different spacers when CuSO₄ was used. Of the DSBs, the C2-capped CuNPs had the highest fluorescence amplification, while the C6-capped CuNPs had the most effective quenching ability (Fig. 13).[105]
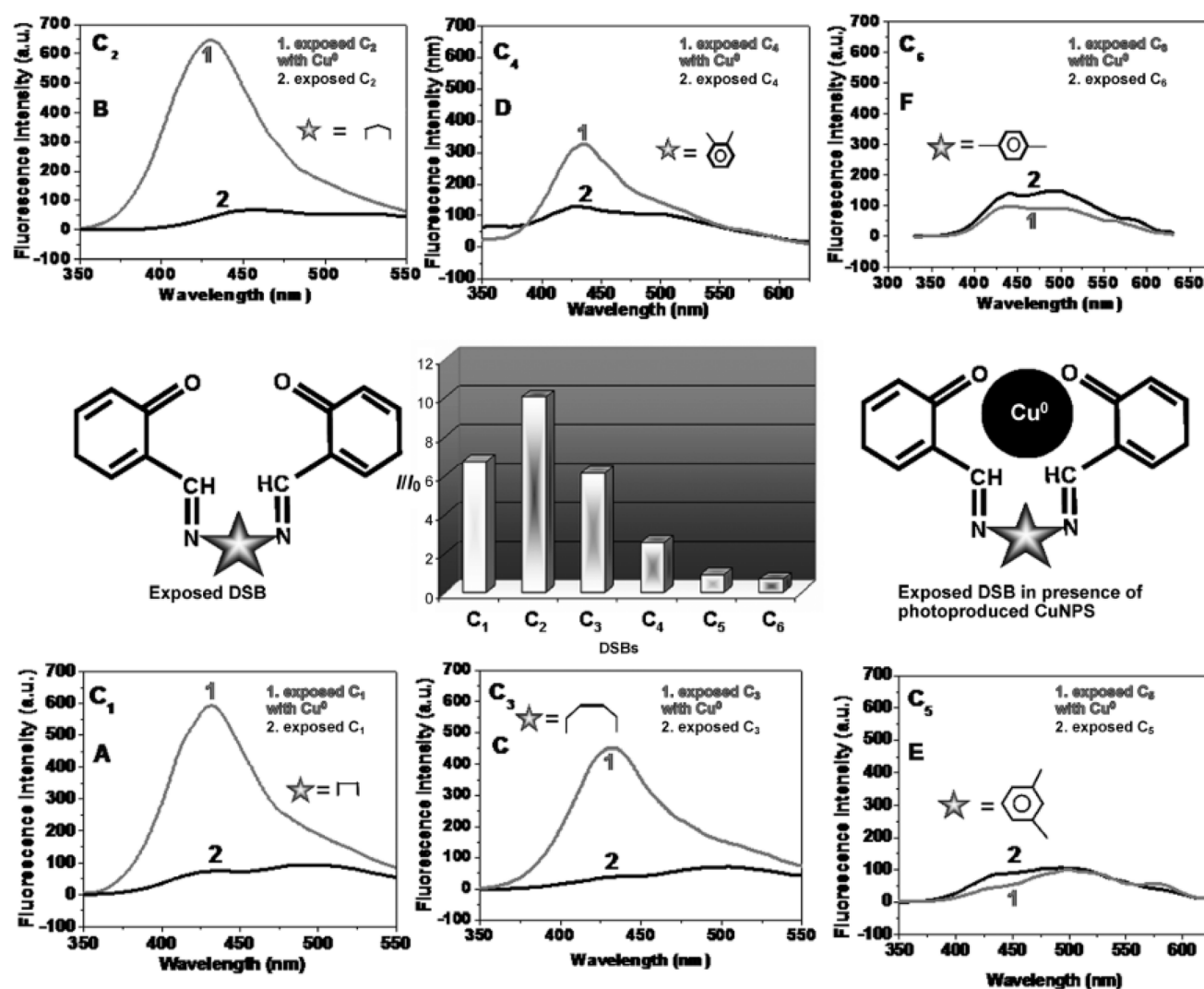

Fig. 13 Fluorescence spectra (A–F) showing enhancement/quenching of exposed DSBs in the presence of photoproduced CuNPs. The bar diagram represents different degrees of enhancement from the exposed DSBs in the presence of photoproduced CuNPs (I = fluorescence intensity of exposed C_2 in the presence of photogenerated CuNPs; I_0 = fluorescence intensity of exposed C2 solution without copper). Reproduced with permission from ref. 105, copyright 2024, *Chem.–Eur. J.*

6.3   Application

6.3.1   Sensing

6.3.1.1   Fluorometric pathway

6.3.1.1.1   Dopamine sensing.
Dopamine (DA) is a catecholamine neurotransmitter that is recognized to be essential in the mammalian central nervous system. A deviation of the usual concentration of dopamine in the brain can lead to Parkinson's disease and other nervous system diseases.[107,112] DA and melamine binding to AuNPs dominated their aptamer-based label-free colorimetric sensing.[113] Rostami et al.[114] designed a colorimetric sensor of DA using hexagonal AgNPs, decorated by the task-specific pyridinium-based ionic liquid.

Ganguly et al. reported on the use of DSB as a fluorophore in the chemosensory detection of dopamine. The fluorescence of DSB-AgNPs was selectively quenched, enabling the detection of DA at nanomolar concentrations. A variety of allied interfering molecules were investigated, including glycine, histidine, isoleucine, leucine, lysine, methionine, phenylalanine, 4-hydroxyproline, serine, threonine, tyrosine, valine, glucose, lactose, Zn^{2+}, and K^+. The DA detection range of 0–300 nM was observed. The LOD was determined to be 16 nM.[107]

As a result, the 3.64 ns lifetime component of the DSB-AgNP solution was changed to 3.97 ns for the DSB-AgNPs-DA solution. This increase in lifetime was an indication of the slightly decreased radiative decay rate. DA-induced fluorescence quenching was quite high, which signified that the decrease of radiative decay was not the major factor for quenching. Therefore, DA effectively trapped the plasmon (lossy surface wave) that radiated as heat and produced ~10 nm AgNPs from highly aggregated microparticles in the DSB-AgNPs. As a result, the scattering cross section was greatly reduced (according to Mie theory) and efficient quenching was observed.[107]

6.3.1.1.2 Hg^{2+} sensing.
One of the most hazardous elements is mercury, and it may be difficult to diagnose low mercury concentrations. Animals and plants as well as people are harmed by mercury. It is discovered that mercury contamination predominantly affects waterways. Gold mining is the main cause of mercury contamination in coastal seas globally, among other sources of the metal. Moreover, fossil fuels are a significant source. The Minamata convention included the formulation of strategies to use less mercury as well as emissions of mercury into the atmosphere.[115,116]

Sahu et al.[117] provided an overview of ionic mercury sensing utilizing AgNPs and AgNCs, both calorimetrically and fluorometrically. Additionally, they demonstrated the need for detection, what happens to analytes and silver particles, how sensing works, actual sample analysis, spot detection for prototype applications, and the impact of adulteration. Kraithong et al. used a tripodal ligand connected to three 7-nitrobenzol-2-oxa-1,3-diazolyl (NBD) molecules (TNBD) to build a selective fluorescence silver-based sensor for Hg^{2+}. This sensor demonstrated good Hg^{2+} selectivity against other interfering ions, with a LOD of 12.5 ppb.[118] For the selective detection of Hg^{2+} and Cu^{2+}, Zhang et al.[119] developed bovine serum albumin-capped fluorescent bimetallic alloying gold–silver NCs.

Hg^{2+} was able to restore the quenched fluorescence (as was mentioned in the dopamine sensing paragraph above) of DSB-AgNPs, caused by DA selectively. Thirteen metal ions were examined in this context: Ba^{2+}, Cd^{2+}, Co^{2+}, K^+, Mg^{2+}, Na^+, Ni^{2+}, Zn^{2+}, Pb^{2+}, Mn^{2+}, Cu^{2+}, Fe^{2+}, Fe^{3+}, and Hg^{2+}. Hg^{2+} alone restored fluorescence due to the complex formation with dopamine. Other interfering basic radials, such as Ba^{2+}, Cd^{2+}, Co^{2+}, K^+, Mn^{2+}, Na^+, Ni^{2+}, Zn^{2+}, and Pb^{2+}, when added separately to AgNPs-dopamine, decreased fluorescence further, while Mn^{2+}, Cu^{2+}, Fe^{2+}, and Fe^{3+} had no influence.[107]

6.3.1.1.3 Ag^+ sensing.
After exposure to UV light for one hour in an $AgNO_3$ + DSB solution, the DSB was oxidized to its semiquinone form. In the vicinity of the oxidized DSB, in situ-produced Ag nanostructures exhibited very efficient MEF. Various basic radicals (Na^+, K^+, Cu^{2+}, Hg^{2+}, Pd^{2+}, Co^{3+}, Cd^{2+}, Ba^{2+}, and Au^{3+}) were used in place of Ag^+ in the same experiment. Ag^+ was the only metal ion that might increase fluorescence. Therefore, silver in an aqueous medium can be detected using DSB as a platform.

It was possible to attain different detection ranges by adjusting the DSB concentrations. The detection ranges were determined to be 0–300 000 nM, 0–250 000 nM, 0–66 000 nM, and 0–22 400 nM, respectively, at concentrations of 2.86×10^{-4} M, 1.43×10^{-4} M, 1.43×10^{-5} M, and 1.43×10^{-6} M.[106]

Ganguly et al.[106] pierced a small hole (0.5 mm diameter) on the pointed edge of a chicken egg, to remove the egg white and yolk. Both the interior semipermeable membrane and the hard egg wall remained intact. Triple-distilled water was used to repeatedly clean the inside of the empty egg membrane. After that, the portion of the hard exterior $CaCO_3$ shell was dissolved from the blunt end in mild HCl to expose the semipermeable membrane within for diffusion testing. The egg membrane and the residual hard shell were retained in a beaker filled with an aqueous alkaline CP solution. Next, the egg cavity was filled with $AgNO_3$ (set 1, quantity of solution). The eggshell with the membrane was then placed in a beaker for a second testing session. This arrangement involved placing the CP solution in the egg cavity and the $AgNO_3$ solution in the beaker (set 2, with the amount of silver being significantly more than CP). For hydrostatic pressure equalization, the solutions (in the hollow and the beaker) stayed at roughly the same height in all of these cases. After three hours, the generation of silver hydroxide caused the colorless silver nitrate solution (sets 1 and 2: internal solution inside the egg membrane and external solution outside the egg membrane) to become blackish brown. After two days, the light yellow solution outside the membrane exhibited less fluorescence intensity than the brown fluid inside the set 1 egg. Set 2 yielded a dark brown solution with reduced light intensity inside the membrane and no fluorescence outside due to the exceptionally high silver concentration. This demonstrated that the silver ion diffused more slowly through the membrane.[12,106]

The experiment of Ganguly et al. demonstrated a useful application of silver-enhanced fluorescence in detecting trace levels of silver ions and provided insightful information on the diffusion dynamics of various compounds through semipermeable membranes. The color variations in the solutions indicated that the silver ions and the CP underwent chemical
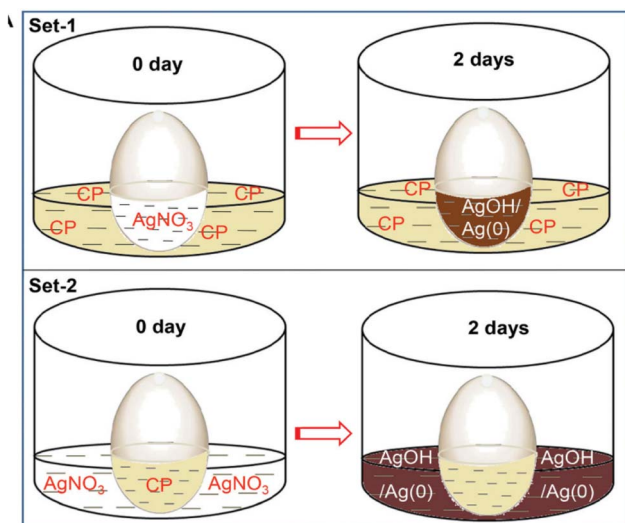
Fig. 14 An illustration of the permeation experiment showing how easily the alkaline CP passed through the egg membrane. Reproduced with permission from ref. 106, copyright 2024, *Dalton Trans.*

reactions. The observed color changes were caused by the creation of silver hydroxide, and the intensity of the fluorescence provided information about the concentration and distribution of silver ions. Variations in the amounts of silver ions and CP were suggested by the differences in fluorescence intensity between the solutions inside and outside the egg membrane. The heightened fluorescence observed within the membrane indicated effective CP transport and subsequent interaction with trace silver ions. The experiment showed how silver-enhanced fluorescence could be used to detect traces of silver in biological systems. Silver ion detection and

quantification, even at low concentrations, had potential applications in biological research and environmental monitoring, among other domains[106] (Fig. 14).

6.4 Fate of DSB-capped coinage metal nanoparticles

Ag^0 $3d_{5/2}$ and $3d_{3/2}$ were represented by the binding energies of 366.21 eV and 372.16 eV, respectively. The peak shift for Ag^0 towards a lower binding energy indicated strict OCP capping. Similarly, Cu^0 $2p_{3/2}$ and Cu^0 $2p_{1/2}$ were represented by the binding energies of 932.74 eV and 952.77 eV. In support of their zero oxidation state, the lattice fringes of AgNPs and CuNPs were measured to be 0.234 and 0.211 nm, respectively [for the (111) plane]. The zero oxidation state of gold was confirmed by the XPS spectra (binding energies of 81.58 eV and 85.19 eV, respectively, corresponding to Au^0 $4f_{7/2}$ and Au^0 $4f_{5/2}$), as well as the lattice fringe (0.236 nm for the (111) plane).[106]

The photoproduced CuNPs capped with exposed C2 had spherical sizes ranging from 3 to 6 nm. Copper was in a zero oxidation state. The peaks at 932.66 and 952.72 eV were assigned to be $2p_{3/2}$ and $2p_{1/2}$, respectively.[105] Ag^+ was reduced to Ag^0, as shown by XPS measurements, XRD, and lattice fringes. The HRTEM scan yielded a lattice fringe of 0.236 nm, which was consistent with the Ag^0 (111) plane. Ag^0 $3d_{5/2}$ and Ag^0 $3d_{3/2}$ were confirmed by ~368.14 and 374.12 eV binding energies, respectively (Fig. 15).[107]

7. Salicylaldehyde-decorated coinage metal nanoclusters

Formally, a metal particle having a diameter of less than 2 nm is called a "nanocluster" (NCs). NCs have shown notable catalytic
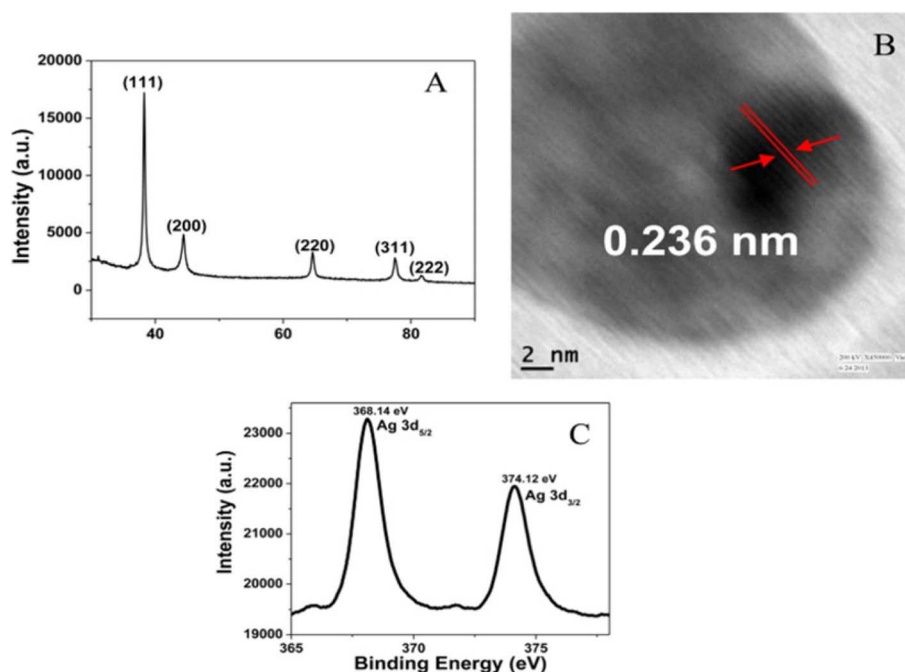

Fig. 15 (A) Powder XRD pattern, (B) lattice fringe, and (C) XPS spectra for the element Ag of DSB capped AgNPs. Reproduced with permission from ref. 107, copyright 2024, *Langmuir.*

activity and unique selectivity in several catalytic processes because of their incredibly small size, abundance of unsaturated active sites, and unique electronic structure that varies from that of ordinary NPs. More importantly, because of their distinct structure and monodispersity, they act as model catalysts to illustrate the connection between atomic-scale structure and catalytic activity. With dimensions typically under 2 nm, noble metal NCs such as silver and gold have attracted attention due to their unique capacity to bridge the "gap" between atomic and NP behavior. Recent research focusing on their quantum electronic properties includes studies on ferromagnetism, chirality, quantum behavior, single molecule optoelectronics, photo-luminescence (PL), bioassay, and sensing. The particle size of NCs is smaller than the exciton Bohr radius, similar to semiconductor quantum dots with tight confinement of the quantum-size range (CdSe quantum dots are 4–5 nm in size).[102,120,121]

The literature contains few reports on SD-conjugated nano-clusters: lysozyme-stabilized AuNCs[122] and trypsin-stabilized AuNCs.[123] The red-emitting AuNCs were stabilized by lyso-zyme, and the trypsin-stabilized AuNCs rapidly changed to yellow and green after the addition of SD. This was due to the formation of an imine linkage between the –CHO group of SD and the –NH$_2$ groups of the lysozyme and trypsin coated on the surface of AuNCs. Zn^{2+} ions could be detected at concentrations as low as 1.37×10^{-7} mM in SD-Lyso-AuNCs, which showed a selective turn-on fluorescence increase at 452 nm. On the other hand, SD-Tryp-AuNCs interacted with Cd^{2+} preferentially and showed a fluorescence enhancement at 660 nm (with a detection limit of 98.1 nM). Sang et al.[124] developed a Schiff base (an aldimine, formed between the aldehyde group of SD and the amino groups of methionine) fluorescent probe based on methionine-protected gold nanoclusters for the detection of Al^{3+}. In the literature, no report is available regarding copper and silver nanoclusters involving SD capping.

The TEM analysis of well-dispersed SD-Tryp-AuNCs revealed that the particles were spherical with a size of approximately 4.8 ± 0.95 nm. The XPS analysis of the SD-Tryp-AuNC survey file revealed peaks for the Au, C, and O atoms. The deconvolution of the C 1s peak produced four binding energy peaks at 284.3, 285.4, 287.7, and 288 eV. The deconvoluted C 1s peaks were attributed to C–C, C=O (carbonyl), COO–, and C=N function-alities, which supported the Schiff base formation between functionalized Tryp and SD. The two peaks at 86.9 eV (Au 4f$_{5/2}$) and 83.3 eV (Au 4f$_{7/2}$) were attributed to the presence of Au metal.[123]

8. Detection of salicylaldehyde

SD is widely used in the chemical industry and environmental processes, making its detection crucial. Naturally, SD is present in buckwheat (Filipendula vulgaris) as an aroma component.[123]

Liu et al.[125] synthesized bovine serum albumin-protected gold nanoclusters (BSA-AuNCs) for the detection of SD. In the presence of fluorescent BSA-AuNCs SD showed enhancement, while no other competitive aldehyde (benzaldehyde, p-nitro-benzaldehyde, and p-dimethylaminobenzaldehyde, and aliphatic aldehydes, such as formaldehyde, glutaraldehyde,

heptaldehyde, and paraformaldehyde) showed such type of enhancement at 500 nm at the same concentration. This finding indicated that the fluorescence switching technique had high selectivity for SD (LOD 0.19 Mm). SD interacted with the BSA-AuNCs, causing two things to happen: the formation of a fluorescent Schiff base due to increased fluorescence, and fluorescence quenching of AuNCs.

9. Conclusions and future perspective

A key component in the production of coinage metal nano-particles with a variety of environmental applications is salicy-laldehyde and its derivatives. These nanoparticles' special qualities make them useful for environmental sensing, catal-ysis, and antibacterial activity. As studies continue, overcoming obstacles and guaranteeing the sustainability of these proce-dures will help salicylaldehyde-derived metal nanoparticles find broad applications in environmental technology. All things considered, the incorporation of environmentally friendly synthesis techniques and the adaptable character of these nanoparticles demonstrate their potential as powerful instru-ments for future environmental concerns.

Salicylaldehyde and its monoiminic and diiminic Schiff bases are used for capping coinage metal nanoparticles. They are used extensively in various sensing applications. However, antibacterial activity is reported for monoiminic Schiff base capped coinage metal nanoparticles. Pure salicylaldehyde and salicylaldehyde-based diiminic Schiff base capped coinage metal particles have not been utilized so far for their antibac-terial activity.

Generation of ultra-small nanoclusters with strong emissive properties (due to inter and intraband transition) is a challenge with finding suitable capping agents and experimental condi-tions. A few reports are available for gold nanocluster formation involving salicylaldehyde. However, copper and silver nano-cluster formation with salicylaldehyde has not been found so far. Owing to the extraordinary demand for fluorescent nano-clusters in analytical and biological science, more research is warranted for the experimental manipulation of salicylaldehyde and its derivatives.

One weak fluorophore and a metal surface (nanoparticles) are needed for MEF, whereas in the case of a cluster, just one entity is needed for the emissive characteristic. Suitable research is required for both cases to enrich the fundamental concept. The position of –OH and –CHO in an aromatic ring is crucial for MEF. Meta-hydroxy benzaldehyde and para-hydroxy benzaldehyde are unable to generate MEF. For the case of dii-minic Schiff bases the spacer between two iminic bonds is responsible for the extent of MEF. Thus, manipulation of MEF can be made possible for prototype applications.

A small molecule exhibiting MEF and manipulation of MEF with its derivatives are the pivotal focus of this review article. This paper is expected to be an asset for the young scientists venturing into the field of nanoscience and nanotechnology from analytical and biological points of view.

Data availability

No data was used for the research described in the article.

Author contributions

Mamta Sahu: writing – original draft; Mainak Ganguly: writing – review & editing, conceptualization; Priyanka Sharma: review & editing.

Conflicts of interest

The authors declare that they have no competing financial interests or personal relationships that could have appeared to influence the work reported in this paper.

References

1 K. A. Maher and S. R. Mohammes, *Int. J. ChemTech Res.*, 2015, **8**, 937–943.
2 M. Das, K. H. Shim, S. S. A. An and D. K. Yi, *Toxicol. Environ. Health Sci.*, 2011, **3**, 193–205.
3 P. Khandel and S. K. Shahi, *J. Nanostruct. Chem.*, 2018, **8**, 369–391.
4 S. Campisi, M. Schiavoni, C. E. Chan-Thaw and A. Villa, *Catalysts*, 2016, **6**, 1–21.
5 Z. Niu and Y. Li, *Chem. Mater.*, 2014, **26**, 72–83.
6 Y. J. Zhuang, J. P. Qu and Y. B. Kang, *J. Org. Chem.*, 2020, **85**, 4386–4397.
7 P. Sharma and M. Ganguly, *New J. Chem.*, 2023, **47**, 7481–7485.
8 M. Sahu, M. Ganguly and A. Doi, *ChemistrySelect*, 2023, **8**, e202301017.
9 Y. Jeong, Y. M. Kook, K. Lee and W. G. Koh, *Biosens. Bioelectron.*, 2018, **111**, 102–116.
10 M. Sui, S. Kunwar, P. Pandey and J. Lee, *Sci. Rep.*, 2019, **9**, 1–14.
11 S. Y. Tee and E. Ye, *Mater. Adv.*, 2021, **2**, 1507–1529.
12 P. Sharma and M. Ganguly, *Int. J. Environ. Sci. Technol.*, 2023, **21**, 3345–3364.
13 N. T. Patil and Y. Yamamoto, *Chem. Rev.*, 2008, **108**, 3395–3442.
14 M. Jin, G. He, H. Zhang, J. Zeng, Z. Xie and Y. Xia, *Angew. Chem. Int. Ed.*, 2011, **50**, 10560–10564.
15 M. Ganguly, J. Pal, S. Das, C. Mondal, A. Pal, Y. Negishi and T. Pal, *Langmuir*, 2013, **29**, 10945–10958.
16 S. Sen and K. Sarkar, *Microb. Drug Resist.*, 2021, **27**, 616–627.
17 M. Sahu, M. Ganguly and A. Doi, *J. Cluster Sci.*, 2024, 1–19.
18 K. B. Borisenko, C. W. Bock and I. Hargittai, *J. Phys. Chem.*, 1996, **100**, 7426–7434.
19 M. Ganguly, A. Pal and T. Pal, *J. Phys. Chem. C*, 2011, **115**, 22138–22147.
20 I. Alata, R. Omidyan, M. Broquier, C. Dedonder and C. Jouvet, *Chem. Phys.*, 2012, **399**, 224–231.
21 A. I. H. Cholilalah and R. Arifin, *J. Math. Chem.*, 1967, **10**, 82–95.
22 T. Stoerkler, D. Frath, D. Jacquemin, J. Massue and G. Ulrich, *Eur. J. Org Chem.*, 2021, **2021**, 3726–3736.
23 A. Karawek, P. Mayurachayakul, T. Santiwat, M. Sukwattanasinitt and N. Niamnont, *J. Photochem. Photobiol., A*, 2021, **404**, 112879.
24 S. Arumugam, B. Shankar and K. C. Mondal, *Eur. J. Inorg. Chem.*, 2020, **2020**, 4127–4136.
25 M. Durko-Maciag, G. Ulrich, D. Jacquemin, J. Mysliwiec and J. Massue, *Phys. Chem. Chem. Phys.*, 2023, 15085–15098.
26 P. Sharma, M. Ganguly and M. Sahu, *Nanoworld J.*, 2023, **9**, 487–495.
27 E. W. F Brühne, *J. Chem. Educ.*, 2005, **82**, 1770.
28 N. R. K. Vilambi and D. -T. Chin, *J. Electrochem. Soc.*, 1987, **134**, 3074–3077.
29 Z. Zhao, L. Zhang, F. Li, X. Tang, Y. Ma, C. Wang, Z. Wang, R. Zhao and L. Wang, *Catalysts*, 2017, **7**, 1–9.
30 M. Sahu, M. Ganguly and P. Sharma, *Spectrochim. Acta, Part A*, 2024, **311**, 123981.
31 M. Ganguly, J. Pal, C. Mondal, A. Pal and T. Pal, *Chem.–Eur. J.*, 2014, **20**, 12470–12476.
32 M. Ganguly, J. Pal, C. Mondal, A. Pal and T. Pal, *Dalton Trans.*, 2015, **44**, 4370–4379.
33 C. D. Geddes, *J. Fluoresc.*, 2002, **12**, 121–129.
34 C. D. Geddes, *Phys. Chem. Chem. Phys.*, 2013, **15**, 19537.
35 M. T. Yaraki and Y. N. Tan, *Chem.–Asian J.*, 2020, **15**, 3180–3208.
36 S. M. Fothergill, C. Joyce and F. Xie, *Nanoscale*, 2018, **10**, 20914–20929.
37 K. Aslan, I. Gryczynski, J. Malicka, E. Matveeva, J. R. Lakowicz and C. D. Geddes, *Curr. Opin. Biotechnol.*, 2005, **16**, 55–62.
38 A. Doi, M. Ganguly and M. Sahu, *Adsorption*, 2024, 1–28.
39 P. Sharma, M. Ganguly and M. Sahu, *RSC Adv.*, 2024, **14**, 11411–11428.
40 S. M. Padre, S. Kiruthika, S. Mundinamani, Ravikirana, S. Surabhi, J. R. Jeong, K. M. Eshwarappa, M. S. Murari, V. Shetty, M. Ballal and S. C. Gurumurthy, *ACS Omega*, 2022, **7**, 35023–35034.
41 F. Zhang, J. Lan, Y. Yang, T. Wei, R. Tan and W. Song, *J. Nanopart. Res.*, 2013, **15**, 1–10.
42 M. R. Willner and P. J. Vikesland, *J. Nanobiotechnol.*, 2018, **16**, 1–16.
43 N. C. Pomal, K. D. Bhatt, K. M. Modi, A. L. Desai, N. P. Patel, A. Kongor and V. Kolivoška, *J. Fluoresc.*, 2021, **31**, 635–649.
44 F. Zarlaida and M. Adlim, *Microchim. Acta*, 2017, **184**, 45–58.
45 D. K. Ban and S. Paul, *Appl. Surf. Sci.*, 2018, **458**, 245–251.
46 K. L. Kelly, E. Coronado, L. L. Zhao and G. C. Schatz, *J. Phys. Chem. B*, 2003, **107**, 668–677.
47 C. Caro, P. M. Castillo, R. Klippstein, D. Pozo and A. P. Zaderenko, *Silver Nanopart.*, 2010, 201–225.
48 W. Chen, S. Cai, Q. Q. Ren, W. Wen and Y. Di Zhao, *Analyst*, 2012, **137**, 49–58.
49 G. He, F. Gao, W. Li, P. Li, X. Zhang, H. Yin, B. Yang, Y. Liu and S. Zhang, *Anal. Methods*, 2019, **11**, 1651–1656.
50 X. Lin, D. Xuan, F. Li, C. Liu, P. Fan, F. Xiao, H. Liang and S. Yang, *Spectrochim. Acta, Part A*, 2020, **229**, 117894.

51 J. Sophia and G. Muralidharan, *Mater. Res. Bull.*, 2015, **70**, 315–320.

52 P. Sharma, M. Ganguly and M. Sahu, *RSC Adv.*, 2024, **14**, 14606–14615.

53 J. Liu, Z. Z. Dong, C. Yang, G. Li, C. Wu, F. W. Lee, C. H. Leung and D. L. Ma, *Sci. Rep.*, 2017, **7**, 4–10.

54 P. Prosposito, L. Burratti and I. Venditti, *Chemosensors*, 2020, **8**, 1–29.

55 S. Bothra, J. N. Solanki and S. K. Sahoo, *Sens. Actuators, B*, 2013, **188**, 937–943.

56 V. D. Doan, T. L. Phan, V. T. Le, Y. Vasseghian, L. O. Evgenievna, D. L. Tran and V. T. Le, *Chemosphere*, 2022, **286**, 131894.

57 S. K. Chandraker, M. Lal, R. Shukla, M. K. Ghosh and T. K. Ghorai, *New J. Chem.*, 2019, **43**, 18175–18183.

58 B. Valeur and I. Leray, *Coord. Chem. Rev.*, 2000, **205**, 3–40.

59 L. Prodi, F. Bolletta, M. Montalti and N. Zaccheroni, *Coord. Chem. Rev.*, 2000, **205**, 59–83.

60 H. T. Ratte, *Environ. Toxicol. Chem.*, 1999, **18**, 89–108.

61 Y. Wen, F. Xing, S. He, S. Song, L. Wang, Y. Long, D. Li and C. Fan, *Chem. Commun.*, 2010, **46**, 2596–2598.

62 J. F. Zhang, Y. Zhou, J. Yoon and J. S. Kim, *Chem. Soc. Rev.*, 2011, **40**, 3416–3429.

63 S. Singha, D. Kim, H. Seo, S. W. Cho and K. H. Ahn, *Chem. Soc. Rev.*, 2015, **44**, 4367–4399.

64 P. K. Mehta, L. N. Neupane, S. H. Park and K. H. Lee, *J. Hazard. Mater.*, 2021, **411**, 125041.

65 M. She, Z. Yang, B. Yin, J. Zhang, J. Gu, W. Yin, J. Li, G. Zhao and Z. Shi, *Dyes Pigm.*, 2012, **92**, 1337–1343.

66 J. L. Bricks, A. Kovalchuk, C. Trieflinger, M. Nofz, M. Büschel, A. I. Tolmachev, J. Daub and K. Rurack, *J. Am. Chem. Soc.*, 2005, **127**, 13522–13529.

67 B. A. Makwana, D. J. Vyas, K. D. Bhatt, V. K. Jain and Y. K. Agrawal, *Spectrochim. Acta, Part A*, 2015, **134**, 73–80.

68 V. K. Gupta, N. Mergu and L. K. Kumawat, *Sens. Actuators, B*, 2016, **223**, 101–113.

69 X. Gao, Y. Lu, S. He, X. Li and W. Chen, *Anal. Chim. Acta*, 2015, **879**, 118–125.

70 E. Weerapana, C. Wang, G. M. Simon, F. Richter, S. Khare, M. B. D. Dillon, D. A. Bachovchin, K. Mowen, D. Baker and B. F. Cravatt, *Nature*, 2010, **468**, 790–797.

71 K. G. Reddie and K. S. Carroll, *Curr. Opin. Chem. Biol.*, 2008, **12**, 746–754.

72 R. Asghar, Y. Li, F. Huo and C. Yin, *Chem. Biomed. Imaging*, 2024, **2**, 250–269.

73 Y. Wang, X. Wang, Q. Meng, H. Jia, R. Zhang, P. Zhu, R. Song, H. Feng and Z. Zhang, *Tetrahedron*, 2017, **73**, 5700–5705.

74 R. Rajamanikandan, B. Aazaad, S. Lakshmipathi and M. Ilanchelian, *Microchem. J.*, 2020, **158**, 105253.

75 Z. Li, J.-T. Hou, S. Wang, L. Zhu, X. He and J. Shen, *Coord. Chem. Rev.*, 2022, **469**, 214695.

76 A. K. Singh, R. Kanchanapally, Z. Fan, D. Senapati and P. C. Ray, *Chem. Commun.*, 2012, **48**, 9047–9049.

77 H.-J. Lee, K.-B. Lee, K.-C. Noh and Y.-S. Nam, *Analyst*, 2015, **140**, 8209–8216.

78 M. Ganguly, J. Jana, C. Mondal, A. Pal and T. Pal, *Phys. Chem. Chem. Phys.*, 2014, **16**, 18185–18197.

79 M. Ganguly, C. Mondal, J. Jana, A. Pal and T. Pal, *Langmuir*, 2014, **30**, 348–357.

80 W. Kang, X. Pei, C. A. Rusinek, A. Bange, E. N. Haynes, W. R. Heineman and I. Papautsky, *Anal. Chem.*, 2017, **89**, 3345–3352.

81 I. V. Anambiga, V. Suganthan, N. Arunai Nambi Raj, G. Buvaneswari and T. S. Sampath Kumar, *Int. J. Sci. Eng. Res.*, 2013, **4**, 710–715.

82 C. M. Da Silva, D. L. Da Silva, L. V. Modolo, R. B. Alves, M. A. De Resende, C. V. B. Martins and Â. De Fátima, *J. Adv. Res.*, 2011, **2**, 1–8.

83 N. Saikumari, *Mater. Today: Proc.*, 2021, **47**, 1777–1781.

84 N. R. Bader, *Rasayan J. Chem.*, 2010, **3**, 660–670.

85 E. Raczuk, B. Dmochowska, J. Samaszko-Fiertek and J. Madaj, *Molecules*, 2022, (3), 787.

86 R. F. Martínez, M. Ávalos, R. Babiano, P. Cintas, J. L. Jiménez, M. E. Light and J. C. Palacios, *Org. Biomol. Chem.*, 2011, **9**, 8268–8275.

87 C. S. Marvel and N. Tarköy, *J. Am. Chem. Soc.*, 1958, **80**, 832–835.

88 G. S. Bhagyasree, B. Nithyaja, V. N. Reena, K. Subin Kumar, T. Shilpa and R. Aswati Nair, *J. Fluoresc.*, 2023, **33**, 1927–1940.

89 A. A. Jimoh, A. Helal, M. N. Shaikh, M. Abdul Aziz, Z. H. Yamani, A. Al-Ahmed and J. P. Kim, *J. Nanomater.*, 2015, **2015**, 101694.

90 V. A. S. Kannaiyan, Easwaramoorthy, K. Kannan and V. Andal, *Nanotechnol. Russ.*, 2020, **15**, 828–836.

91 F. A. Almashal, Z. T. Al-Abdullah and A. M. Jassem, *Egypt. J. Chem.*, 2020, **63**, 813–821.

92 P. Sharma, M. Ganguly and A. Doi, *Appl. Nanosci.*, 2024, **14**, 739–751.

93 M. Sankarganesh, P. Adwin Jose, J. Dhaveethu Raja, M. P. Kesavan, M. Vadivel, J. Rajesh, R. Jeyamurugan, R. Senthil Kumar and S. Karthikeyan, *J. Photochem. Photobiol., B*, 2017, **176**, 44–53.

94 N. O. Mahmoodi, N. Aghajani and A. Ghavidast, *J. Mol. Struct.*, 2017, **1128**, 21–29.

95 S. S. Alharthi, T. Gomathi, J. John Joseph, J. Rakshavi, J. Annie Kamala Florence, P. N. Sudha and G. Rajakumar, *J. King Saud Univ., Sci.*, 2022, **34**, 102177.

96 J. R. Lakowicz, *Anal. Biochem.*, 2005, **337**, 171–194.

97 M. Sahu, A. Kumar Manna, K. Rout, J. Mondal and G. K. Patra, *Inorg. Chim. Acta*, 2020, **508**, 119633.

98 A. K. Manna, J. Mondal, R. Chandra, K. Rout and G. K. Patra, *J. Photochem. Photobiol., A*, 2018, **356**, 477–488.

99 T. Gong, J. Liu, X. Liu, J. Liu, J. Xiang and Y. Wu, *Food Chem.*, 2016, **213**, 306–312.

100 S. Tang and J. Zheng, *Adv. Healthcare Mater.*, 2018, **7**, 1–10.

101 C. Su, K. Huang, H.-H. Li, Y. G. Lu and D. L. Zheng, *J. Nanomater.*, 2022, **2020**, 5616379.

102 M. Sahu, M. Ganguly and P. Sharma, *Nanoworld J.*, 2023, **9**, 496–504.

103 M. F. Al-Hakkani, *SN Appl. Sci.*, 2020, **2**, 505.

104 A. Mobed, M. Hasanzadeh and F. Seidi, *RSC Adv.*, 2021, **11**, 34688–34698.

105 M. Ganguly, A. Pal, Y. Negishi and T. Pal, *Chem.–Eur. J.*, 2012, **18**, 15845–15855.

106 M. Ganguly, C. Mondal, J. Chowdhury, J. Pal, A. Pal and T. Pal, *Dalton Trans.*, 2014, **43**, 1032–1047.

107 M. Ganguly, C. Mondal, J. Jana, A. Pal and T. Pal, *Langmuir*, 2014, **30**, 4120–4128.

108 J. R. Lakowicz, C. D. Geddes, I. Gryczynski, J. Malicka, Z. Gryczynski, K. Aslan, J. Lukomska, E. Matveeva, J. Zhang, R. Badugu and J. Huang, *J. Fluoresc.*, 2004, **14**, 425–441.

109 I. Gryczynski, J. Malicka, Y. Shen, Z. Gryczynski and J. R. Lakowicz, *J. Phys. Chem. B*, 2002, **106**, 2191–2195.

110 J. R. Lakowicz, Y. Shen, S. D'Auria, J. Malicka, J. Fang, Z. Gryczynski and I. Gryczynski, *Anal. Biochem.*, 2002, **301**, 261–277.

111 K. Sokolov, G. Chumanov and T. M. Cotton, *Anal. Chem.*, 1998, **70**, 3898–3905.

112 R. M. Wightman, L. J. May and A. C. Michael, *Anal. Chem.*, 1988, **60**, 769–779.

113 X. Liu, F. He, F. Zhang, Z. Zhang, Z. Huang and J. Liu, *Anal. Chem.*, 2020, **92**, 9370–9378.

114 S. Rostami, A. Mehdinia, A. Jabbari, E. Kowsari, R. Niroumand and T. J. Booth, *Sens. Actuators, B*, 2018, **271**, 64–72.

115 M. Liu, Q. Zhang, T. Maavara, S. Liu, X. Wang and P. A. Raymond, *Nat. Geosci.*, 2021, **14**, 672–677.

116 A. C. (Thanos) Bourtsalas and N. J. Themelis, *Waste Manage.*, 2019, **85**, 90–94.

117 M. Sahu, M. Ganguly and P. Sharma, *RSC Adv.*, 2024, **14**, 22374–22392.

118 S. Kraithong, N. Chailek, J. Sirirak, K. Suwatpipat, N. Wanichacheva and P. Swanglap, *J. Photochem. Photobiol., A*, 2021, **407**, 113064.

119 N. Zhang, Y. Si, Z. Sun, L. Chen, R. Li, Y. Qiao and H. Wang, *Anal. Chem.*, 2014, **86**, 11714–11721.

120 H. Huang, H. Li, J. J. Feng, H. Feng, A. J. Wang and Z. Qian, *Sens. Actuators, B*, 2017, **241**, 292–297.

121 G.-X. Duan, Y.-P. Xie, Y.-L. Shen, X. Lu, J. Han and L.-P. Zhang, *Mater. Chem. Front.*, 2020, **4**, 2205–2222.

122 V. Bhardwaj, T. Anand, H. J. Choi and S. K. Sahoo, *Microchem. J.*, 2019, **151**, 104227.

123 A. Tripathi, V. Bhardwaj and S. K. Sahoo, *J. Fluoresc.*, 2023, 1–9.

124 H. Shi, Y. Zhao, F. Sang, T. Xiong, W. Wang and J. Pan, *J. Fluoresc.*, 2022, **33**, 177–184.

125 X. Liu, C. Fu, X. Ren, H. Liu, L. Li and X. Meng, *Biosens. Bioelectron.*, 2015, **74**, 322–328.